

Explaining the Equatorial Pacific Thermocline Response to Climate Change with a Model Hierarchy

Matthew T. Luongo^{1,2*}, Shang-Ping Xie³, Ian Eisenman³, Shantong Sun⁴, & Kyle Armour^{2,5}

1. Cooperative Institute for Climate, Ocean, & Ecosystem Studies, University of Washington, Seattle, WA, USA
2. School of Oceanography, University of Washington, Seattle, WA, USA
3. Scripps Institution of Oceanography, UC San Diego, La Jolla, CA, USA
4. Laoshan Laboratory, Qingdao, China
5. Department of Atmospheric & Climate Science, University of Washington, Seattle, WA, USA

* mluongo@uw.edu

This manuscript is a pre-print submitted to EarthArXiv.

The pre-print has been submitted for review to *Journal of Geophysical Research: Oceans*.

Subsequent versions may have altered content.

Explaining the Equatorial Pacific Thermocline Response to Climate Change with a Model Hierarchy

Matthew T. Luongo^{1,2}, Shang-Ping Xie³, Ian Eisenman³, Shantong Sun⁴, &
Kyle C. Armour^{2,5}

¹Cooperative Institute for Climate, Ocean, & Ecosystem Studies, University of Washington, Seattle, WA

²School of Oceanography, University of Washington, Seattle, WA

³Scripps Institution of Oceanography, UC San Diego, La Jolla, CA

⁴Laoshan Laboratory, Qingdao, China

⁵Department of Atmospheric & Climate Science, University of Washington, Seattle, WA

Key Points:

- Climate models can largely recreate observed equatorial Pacific subsurface temperature trends from 1958-2020
- The observed subsurface temperature change is due to wind changes, remote SST changes, and local SST changes
- Our results suggest that canonical drivers of the equatorial Pacific response to climate change have been misattributed

Corresponding author: M.T. Luongo, mluongo@uw.edu

Abstract

17 Most studies of the equatorial Pacific response to anthropogenic forcing have focused on
18 patterns of sea surface temperature (SST) change. However, similar SST patterns can
19 be consistent with a range of different subsurface responses, each with differing physi-
20 cal and biogeochemical implications. While historical observation and climate model mis-
21 matches have been suggested in the literature, we show that model simulations can largely
22 capture the observed 1958-2020 subsurface temperature trend in the equatorial thermo-
23 cline. We then analyze a hierarchy of idealized model simulations, consisting of fully-coupled,
24 mechanically-decoupled, ocean-only, and reduced gravity models, to understand which
25 ocean dynamics contribute to this response. We show that the response of the thermo-
26 cline to idealized climate change can be explained by a combination of decadal momen-
27 tum dynamics and radiatively-forced buoyancy-driven dynamics. We further decompose
28 the buoyancy-driven pattern into a pattern driven by remote, subtropical SST forcing
29 and a pattern driven by local, equatorial SST forcing. The remote-SST-forced pattern
30 of thermocline warming shows the signature of dynamic and thermodynamic subtrop-
31 ical cell adjustments. Meanwhile, increased stratification in the local-SST-forced pattern
32 both coherently shoals the thermocline and relaxes thermocline tilt to largely cool the
33 thermocline. Considered together, we recreate the long-term subsurface equatorial Pa-
34 cific response to idealized greenhouse gas forcing as a linear combination of (i) wind-stress-
35 driven changes, (ii) remote buoyancy-driven changes, and (iii) local buoyancy-driven changes.
36 To conclude we discuss implications for recent temperature trends, revisit canonical the-
37 ories of the ocean dynamical thermostat, and show the insensitivity of forced responses
38 to forcing geography.
39

Plain Language Summary

41 While most research on the equatorial Pacific response to climate change has fo-
42 cused on surface ocean temperatures, ocean circulation changes provide insight into the
43 dynamic drivers of that response. For instance, though eastern equatorial Pacific sur-
44 face cooling could result from either strengthening winds or subsurface communication
45 of subtropical cooling, these mechanisms affect the subsurface distinctly. In this work
46 we first show that climate model simulations can largely capture the observed 1958-2020
47 equatorial Pacific subsurface temperature response to climate change. We then use a se-
48 ries of idealized modeling simulations, from a complex global climate model to a sim-

49 ple primitive equation model, to explain the ocean dynamics that create this response.
50 Our central result is that the equatorial Pacific subsurface temperature response to cli-
51 mate change is a simple linear sum of the ocean’s response to changes in winds, changes
52 in remote sea surface temperature patterns, and changes in local sea surface tempera-
53 ture patterns. We explore the dynamics of each of these individual responses. Last, we
54 show that this understanding does not explain subsurface temperature patterns since the
55 late 1970s, and we discuss how our results suggest a reinterpretation of how certain ocean
56 dynamics shape the equatorial ocean’s response to climate change.

57 **1 Introduction**

58 A strong zonal gradient in sea surface temperature (SST) exists in the equatorial
59 Pacific between the western Pacific warm pool and the eastern Pacific cold tongue. This
60 zonal SST gradient is the most obvious manifestation of a series of coupled atmospheric
61 and oceanic processes that connect easterly trade winds, westward surface currents, an
62 eastward subsurface return flow within an upward tilting thermocline, and upwelling of
63 cool sub-thermocline waters in the eastern equatorial Pacific (Bjerknes, 1969; Wyrтки,
64 1975). Variability in the equatorial Pacific mean state shifts the location of atmospheric
65 deep convection and excites planetary waves that propagate to the extratropics to af-
66 fect global climate (Horel & Wallace, 1981). Across a broad range of time-scales, from
67 interannual changes of the El Niño-Southern Oscillation (ENSO, Philander, 1983) to decadal
68 changes of the Pacific Decadal Oscillation (PDO, Mantua et al., 1997), the equatorial
69 Pacific is a key driver and pacemaker for global climate (e.g., Kosaka & Xie, 2016).

70 Given its outsize influence on Earth’s climate, it is critical to understand how the
71 equatorial Pacific will respond to anthropogenic greenhouse gas emissions (e.g., DiNezio
72 et al., 2009; Xie et al., 2010). A key question, which has received much attention and
73 debate, is: How will the equatorial zonal SST gradient change in the future? Constraints
74 from atmospheric thermodynamics have been primarily invoked in support of a decreas-
75 ing gradient (i.e., more warming in the eastern than western equatorial Pacific): enhanced
76 evaporative cooling in the warmer western Pacific can more readily balance anomalous
77 radiative forcing than the cooler eastern Pacific (Knutson & Manabe, 1995; Merlis & Schnei-
78 der, 2011), and the atmospheric Walker circulation slow-down implied by specific humid-
79 ity changes would relax thermocline tilt (Vecchi & Soden, 2007). Meanwhile, Clement
80 et al. (1996) and Seager and Murtugudde (1997) proposed the “ocean dynamical ther-

81 mostat” and suggested that the zonal SST gradient should in fact increase. The ther-
82 mostat theory suggests that the eastern equatorial Pacific should warm by less than the
83 rest of the tropics because upwelled equatorial waters, originating in the extratropics and
84 reaching the equator via the oceanic subtropical cells (STCs: Liu, 1994; McCreary Jr &
85 Lu, 1994), will not show an effect of surface forcing until some time later. More recently,
86 several studies have suggested that this debate is simply a matter of time-scales, with
87 a brief strengthening of the zonal gradient eventually giving way to a long-term weak-
88 ening (Luo et al., 2017; Heede et al., 2020, 2021; Heede & Fedorov, 2021).

89 However, the continued inability of coupled models to recreate recent historical equa-
90 torial Pacific SST trends (Coats & Karnauskas, 2017; Seager et al., 2019, 2022; Watan-
91 abe et al., 2021; Wills et al., 2022) calls into question this seeming resolution. While ob-
92 servational products suggest that the western Pacific has warmed and central-eastern Equa-
93 torial Pacific has cooled since the beginning of the satellite era (e.g., Karnauskas et al.,
94 2009; Solomon & Newman, 2012; Seager et al., 2019; Wills et al., 2022), over that same
95 period the vast majority of coupled global climate models (GCMs) show enhanced warm-
96 ing in the eastern Pacific relative to the western Pacific. Many studies have attempted
97 to explain the mismatch between observed and modeled equatorial Pacific SST trends,
98 pointing to i) mismatched internal variability (e.g., Laepple & Huybers, 2014; Olonscheck
99 et al., 2020; Watanabe et al., 2021; Heede & Fedorov, 2023; Sweeney et al., 2023; Jiang
100 et al., 2024a), ii) incorrect model processes that could otherwise create observed trends
101 (e.g., McGregor et al., 2018; Baldwin et al., 2021; Dong et al., 2022; Kang et al., 2023;
102 Hwang et al., 2024), and iii) systematic biases in model mean states that do not allow
103 a forced response to establish (Seager et al., 2019, 2022; Heede & Fedorov, 2023; Jiang
104 et al., 2024a, 2025).

105 While the mismatch between observed and modeled historical equatorial SST has
106 been extensively discussed, the subsurface equatorial temperature response to climate
107 change has been relatively understudied. This top-down focus on SST alone potentially
108 obfuscates important subsurface oceanic adjustments (e.g., Clement et al., 1996; Vec-
109 chi & Soden, 2007) that have helped to shape the SST response. For instance, despite
110 comprising entirely different subsurface dynamics, both decreased thermocline tilt (Vecchi
111 & Soden, 2007; Luongo et al., 2023) and coherent thermocline deepening (Luongo et al.,
112 2025) could theoretically lead to an El Niño-like SST pattern.

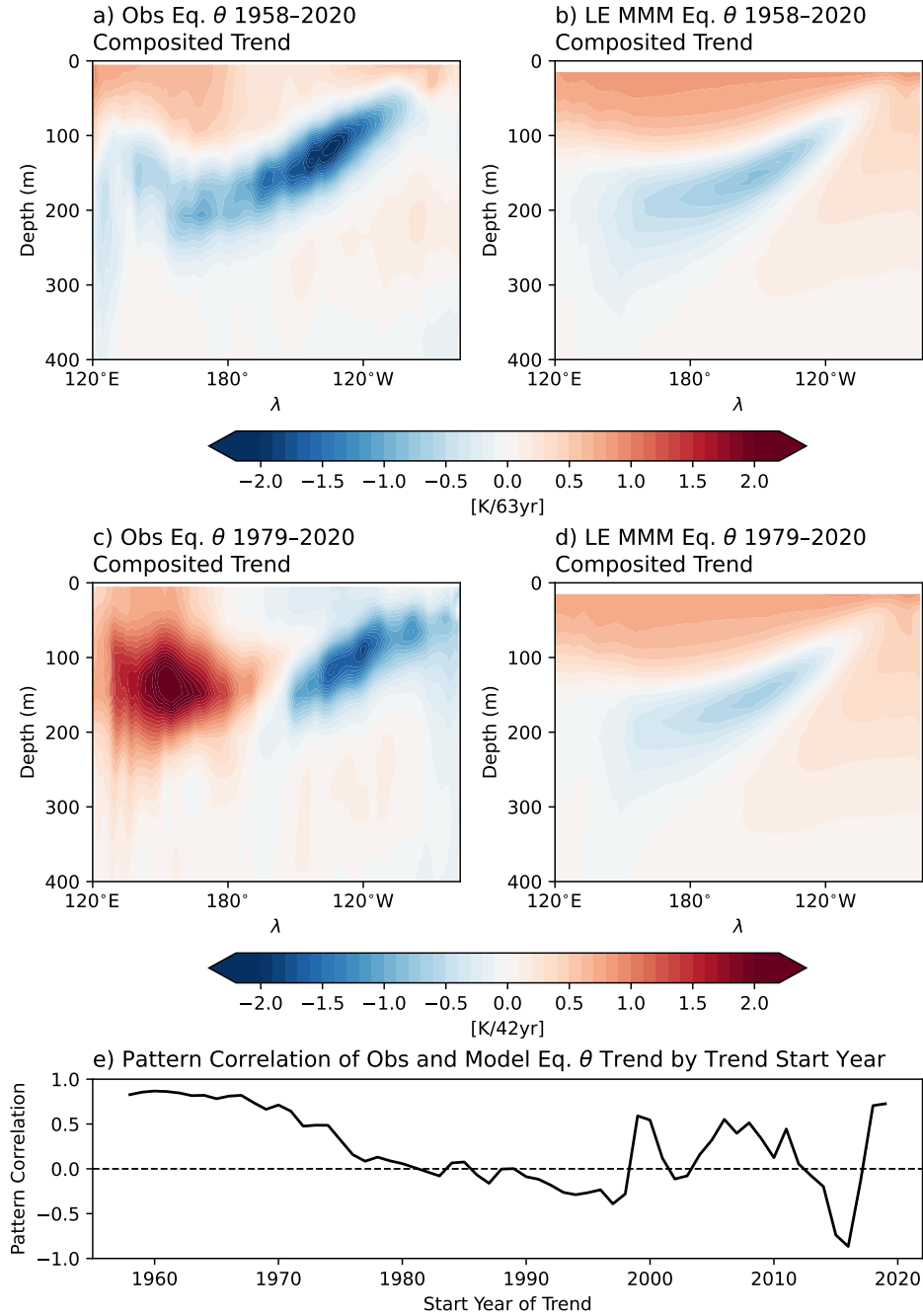


Figure 1. a) 1958-2020 annual-mean equatorial temperature (θ) trend composited from EN04 and Ishii observational products and ORAS5 and SODA2.2.4 reanalyses. b) Multi-model mean equatorial θ from 11 large ensemble simulations over 1958-2020. c) As in panel a) but for the period of 1979-2020. d) As in panel b) but for the period of 1979-2020. e) Pearson pattern correlation between observational and multi-model mean equatorial θ trend as a function of trend start year.

113 Following Jiang et al. (2025), we show a composite of the 1958-2020 subsurface equa-
114 torial (meridionally averaged from 5°S-5°N) Pacific temperature trend from two obser-
115 vational products [EN04 (1958-2020, Good et al., 2013) & Ishii (1958-2012, Ishii & Ki-
116 moto, 2009)] and two ocean reanalyses [ORAS5 (1958-2020, Zuo et al., 2019) & SODA2.2.4
117 (1958-2010, Carton & Giese, 2008)] (Figure 1a). The most obvious feature of subsurface
118 equatorial temperatures over the past 60 years is a broad thermocline cooling. Due to
119 the upward and eastward tilt of the thermocline, this cooling is around 250m deep in the
120 west-central Pacific and around 50m deep in the eastern Pacific. Maximum cooling oc-
121 curs between 150°W-120°W from approximately 100-175m. While the cooling is the most
122 eye-catching feature in this observational pattern, we also note a broad surface warm-
123 ing, which is minimized in the central Pacific and extends deeper in the western Pacific
124 than eastern Pacific, and a sub-thermocline warming in the eastern Pacific. These fea-
125 tures are largely shared by individual observational products (Figure S1).

126 The observed 1958-2020 subsurface temperature trend in Figure 1a is similar to the
127 1951-2010 trend pattern in Watanabe et al. (2021). We note, however, that the specific
128 time period considered greatly influences this pattern: Figure 1a is markedly different
129 than both the 1979-2020 pattern (Figure 1c) and the 1979-2013 pattern (Watanabe et
130 al., 2024). The observed trend over this shorter period features a striking zonal temper-
131 ature dipole, western Pacific warming and the eastern Pacific cooling, within the top 200m.
132 This temperature dipole dynamically agrees with the upper ocean circulation strength-
133 ening noted by Tuchen et al. (2024) over the overlapping period of 1993-2022.

134 In a series of recent studies inspired by Seager et al. (2019)'s hypothesis that the
135 models' mean state ocean is simply too biased to capture observed SST trends, Jiang
136 et al. (2024a, 2024b, 2025) highlight the differences in the subsurface trend patterns be-
137 tween observations and models. In particular, the authors hypothesize that the observed
138 subsurface cooling response can be explained as a forced response to wind changes (Jiang
139 et al., 2024a, 2024b) and that models lack an effective connectivity between subsurface
140 and surface eastern Pacific temperatures due to insufficient upwelling and mixing (Jiang
141 et al., 2025). However, the corresponding 1958-2020 subsurface temperature trend com-
142 posite from a suite of 11 large ensemble simulations from the sixth coupled model inter-
143 comparison project [Figure 1b, inspired by Jiang et al. (2025)] shows a similar pattern
144 to observations (Figure 1a; Pearson pattern correlation of 0.83). Both show a broad ther-
145 mocline cooling, a somewhat zonally symmetric surface warming, and a sub-thermocline

146 eastern Pacific warming. Indeed, despite model biases, there is general agreement be-
147 tween observed and modeled subsurface temperature trends when those trends begin be-
148 fore ~ 1975 (Figure 1e), suggesting that the modeled subsurface temperature trend can
149 still inform our understanding of the observed subsurface temperature trend and the cou-
150 pled dynamics that have created it. This perspective motivates the central questions of
151 our study: 1) which ocean dynamics contribute to this common modeled response, and
152 2) to what extent is the full response a simple linear combination of these responses?

153 A handful of studies have explored the models' shared central-western Pacific ther-
154 mocline cooling response (c.f. Figure 1b and Figure S2) which has persisted for several
155 model generations. Vecchi and Soden (2007) suggest that this cooling is a local effect
156 caused by a reduction in thermocline tilt due to a weaker atmospheric Walker circula-
157 tion. Yang et al. (2009) suggest that this weaker Walker circulation slows down the STCs
158 and dynamically cools the equatorial subsurface. Luo et al. (2009, 2018) agree that mod-
159 els' STCs have slowed, but suggest that a major cause of the slowdown is increased sub-
160 tropical surface stratification. Finally, Ju et al. (2022) suggest that the cooling is caused
161 by mean advection of density-compensated spiciness anomalies from the subtropics, which
162 cool the region as much as dynamical changes in subtropical cell circulation.

163 While these studies provide a starting point for answering our guiding questions,
164 it's evident that these proposed mechanisms are entwined with murky causality. A com-
165 mon means of circumventing the attribution issues common to coupled dynamics is to
166 employ a model hierarchy to step through a complex response by iteratively removing
167 complexity until the phenomenon of interest is isolated. For instance, recent studies have
168 overrode surface wind stress to mechanically decouple a GCM's ocean from its atmosphere
169 (e.g., Luongo et al., 2024) and have shown that the ocean's full response to an anoma-
170 lous forcing can be linearly partitioned into the response due to anomalous surface buoy-
171 ancy forcing and anomalous surface momentum forcing (Luongo et al., 2022, 2023). Sim-
172 ilarly, ocean-only GCM (OGCM) simulations are a convenient way to isolate just the ocean's
173 response to a forcing without changes in the atmosphere (e.g., Peng et al., 2022).

174 In this study we employ a model hierarchy, consisting of a fully-coupled GCM, a
175 mechanically-decoupled GCM, an OGCM, and a primitive equation reduced gravity model,
176 to explore the modeled subsurface equatorial Pacific temperature response to greenhouse
177 gas forcing and which ocean dynamics contribute to it. We discuss the simulations that

178 comprise this hierarchy in section 2 and in section 3 we show that the full response can
179 be understood as a linear sum of the response due to i) momentum effects, ii) remote
180 buoyancy effects, and iii) local buoyancy effects. We discuss implications of these results
181 in section 4 and we conclude in section 5.

182 **2 Model Hierarchy**

183 All simulations used to explore the equatorial Pacific thermocline response to green-
184 house gas forcing are presented in Table 1. Simulations that explore the equatorial Pa-
185 cific thermocline response to non-greenhouse-gas forcing schemes are presented in Ta-
186 ble S1.

187 **2.1 Fully-Coupled Simulations**

188 We analyze pre-existing simulations using the National Center for Atmospheric Re-
189 search’s Community Earth System Model, Version 1.2 (CESM1: Hurrell et al., 2013) that
190 were initially presented in Luongo et al. (2022) and Taylor et al. (2025). These simula-
191 tions have a nominal horizontal resolution of 2° in the atmosphere and land components
192 and 1° in the ocean and sea ice components, though the oceanic component has higher
193 resolution near the equator to better resolve equatorial dynamics. They are run in a stan-
194 dard coupled configuration with pre-industrial forcing (“B1850” compset) for fifty years.

195 Our preindustrial control (Ctrl) simulation extends directly from initialization with
196 no anomalous forcing applied. To idealize climate change we apply and maintain an abrupt
197 quadrupling of CO_2 relative to pre-industrial levels ($\text{CO}_2 \times 4$). While abrupt quadrupling
198 of CO_2 is an obvious simplification compared to a more realistic time-evolving increase
199 in CO_2 , we show in section 3.1 that this idealization works remarkably well. While we
200 primarily focus on the equatorial Pacific’s response to greenhouse gas forcing in this study,
201 we also consider simulations with hemispherically asymmetric forcing to test how robust
202 the ocean dynamics of interest are to forcing geometry. We apply a zonally-uniform top-
203 of-atmosphere (TOA) insolation reduction following the Extratropical-Tropical Interac-
204 tion Model Intercomparison Project (ETINMIP: Kang et al., 2019) protocol in the North-
205 ern Hemisphere (NH, 45°N - 65°N) for ETINMIPNH and in the Southern Hemisphere (SH,
206 45°S - 65°S) for ETINMIPSH. The ETINMIP forcing corresponds to an annual-mean, zonal-
207 mean forcing of approximately -45 Wm^{-2} at 55° N or S and falls off as an approximate

| Fully-coupled Simulations | | |
|------------------------------------|---|------------------------|
| Simulation Name | CO ₂ Forcing | Wind Stress |
| Ctrl | 280ppm | Freely evolving |
| CO ₂ x4 | 1120ppm | Freely evolving |
| Mechanically-decoupled Simulations | | |
| Simulation Name | CO ₂ Forcing | Wind Stress |
| Tau1CO ₂ x1 | 280ppm | Ctrl |
| Tau1CO ₂ x4 | 1120ppm | Ctrl |
| Tau4CO ₂ x1 | 280ppm | CO ₂ x4 |
| Ocean-only Simulations | | |
| Simulation Name | SST Forcing Perturbation | SST Forcing Bounds |
| OCtrl | n/a | n/a |
| CO ₂ x4.BFsst | Tau1CO ₂ x4-Tau1CO ₂ x1 | 90°S-90°N |
| CO ₂ x4.BFsstET | Tau1CO ₂ x4-Tau1CO ₂ x1 | 90°S-6°S, 6°N-90°N |
| CO ₂ x4.BFsstEQ | Tau1CO ₂ x4-Tau1CO ₂ x1 | 10°S-10°N |
| NEPac2CWarm | +2°C | 147°W-123°W, 22°N-32°N |
| Reduced Gravity Simulations | | |
| Simulation Name | Reduced Gravity | |
| RGCtrl | 1x | |
| RGx2 | 2x | |

Table 1. Details of the fully coupled, mechanically-decoupled, ocean-only, and reduced-gravity simulations used to study the equatorial Pacific thermocline response to greenhouse gas forcing. Table S1 presents simulations that explore alternate forcing schemes.

208 Gaussian. For all CESM1 simulations we consider an average over years 11-50 after the
 209 forcing is applied as in Luongo et al. (2022, 2023).

210 **2.2 Mechanically-Decoupled Simulations**

211 We perform wind stress overriding simulations (e.g., Luongo et al., 2024) to iso-
 212 late the dynamic effect of buoyancy and momentum flux anomalies on the ocean, while
 213 still maintaining some amount of realistic atmosphere-ocean coupling. In a fully-coupled
 214 simulation the coupler interactively provides the ocean component with atmospheric wind
 215 stress. This momentum flux coupling then drives changes in the ocean state (e.g., equa-
 216 torial thermocline tilt which changes the zonal SST gradient), which can then feed back
 217 on the atmosphere in the next coupling step (e.g., Bjerknes feedback). In wind stress over-
 218 riding simulations, however, the GCM is instead modified to receive a known surface wind
 219 stress field, disabling the interactive coupling of momentum fluxes and mechanically de-
 220 coupling the ocean from the atmosphere. All other coupling, including the effect of wind
 221 speed on turbulent heat fluxes, remain in tact.

222 In our mechanically-decoupled simulations we either apply a radiative forcing (CO_2
 223 quadrupling or ETINMIP TOA forcing) and lock to Ctrl’s wind stress field, or we ap-
 224 ply no radiative forcing but we lock to a perturbed simulation’s wind stress field. For
 225 example, we perform a simulation where we abruptly quadruple CO_2 , but we override
 226 with unperturbed Ctrl wind stress ($\text{Tau1CO}_2\text{x4}$). This simulation highlights the radiatively-
 227 driven climate response because wind stress is unperturbed. We also perform a simu-
 228 lation where we apply no CO_2 forcing, but we override with the perturbed wind stress
 229 field from $\text{CO}_2\text{x4}$ to highlight the climate response just due to wind stress ($\text{Tau4CO}_2\text{x1}$).
 230 Similarly, we perform a simulation where we apply a reduction in insolation in the NH
 231 following the ETINMIP protocol described above, but we override with unperturbed Ctrl
 232 wind stress ($\text{Tau}_1\text{S_NH}$), and we perform a simulation where we apply no insolation
 233 reduction, but we override with the perturbed wind stress field from ETINMIPNH (Tau_NH_S_1).
 234 $\text{Tau}_1\text{S_SH}$ and Tau_SH_S_1 are similar, but correspond to the SH ETINMIP simula-
 235 tions.

236 In these wind overriding simulations we prescribe the full interannually-varying wind
 237 stress field to maintain the impact of high-frequency mechanical variability on the sur-
 238 face ocean and reduce mean state biases (Luongo et al., 2024). Finally, in order to re-
 239 move mean state biases introduced by the mechanical decoupling technique, we compare

240 these perturbed mechanically-decoupled simulations to a control mechanically-decoupled
 241 simulation (Tau1CO₂x1), which has no radiative forcing and wind stress locked to Ctrl.
 242 As such, our buoyancy-forced (BF) response is Tau1CO₂x4-Tau1CO₂x1 and our momentum-
 243 forced (MF) response is Tau4CO₂x1-Tau1CO₂x1. See discussion in Luongo et al. (2022,
 244 2023, 2024) for more detail on this protocol.

245 **2.3 Ocean-only Simulations**

246 We use an ocean-only version of the Massachusetts Institute of Technology Gen-
 247 eral Circulation Model (MITgcm) in the same configuration used in Luongo et al. (2025),
 248 which is similar to the Estimated the Circulation and Climate of the Ocean version 4
 249 release 4 (ECCOv4r4: Forget et al., 2015) configuration. This OGCM has 1° horizon-
 250 tal resolution in the zonal direction and 1/3° meridional resolution at high and low lat-
 251 itudes (telescoping to 1° in midlatitudes). While not fully permitting high latitude mesoscale
 252 eddies, the higher resolution in the equatorial region begins to resolve equatorial waves
 253 and thus decrease tropical biases. This MITgcm configuration is forced with monthly
 254 climatologies of net air-sea fluxes of heat, freshwater, shortwave radiation, and zonal and
 255 meridional momentum diagnosed by Peng et al. (2022) from a 25-year control integra-
 256 tion of ECCOv4r4 with bulk formulae forcing. In addition to climatological flux forc-
 257 ing, we restore SST and sea surface salinity to Peng et al. (2022)’s climatologies on a 10-
 258 day timescale. All of our OGCM simulations branch from a 100-year spin-up, at which
 259 point the upper-ocean is approximately equilibrated. See Luongo et al. (2025) for fur-
 260 ther details.

261 Our OGCM control simulation (OCtrl) is integrated for 30 years. We also perform
 262 a series of perturbation experiments where we add the anomalies in the BF SST field di-
 263 agnosed from our mechanically-decoupled CESM1 simulations to the SST relaxation field.
 264 We add anomalies in the quasi-equilibrium (average over years 11-50) SST field calcu-
 265 lated from Tau1CO₂x4-Tau1CO₂x1, Tau_1_S_NH-Tau1CO₂x1, and Tau_1_S_SH-Tau1CO₂x1
 266 (producing ocean-only simulations CO₂x4_BFsst, ETINMIPNH_BFsst, and ETINMIPSH_BFsst,
 267 respectively). Comparing these SST-forced perturbation experiments with OCtrl shows
 268 the ocean-only dynamic response to the buoyancy-driven SST response. Because any tem-
 269 perature response within the first few depth levels is more likely to be driven by the strong
 270 surface relaxation than by a dynamical adjustment, we focus our discussion of the dy-
 271 namics revealed by the OGCM simulations on the thermocline and below.

272 Finally, we split these perturbation experiments geographically into SST forcing
 273 from only the extratropical regions and SST forcing from only the equatorial region (“ET”
 274 or “EQ” appended to above names). In the extratropical SST forcing experiment we ap-
 275 ply the full CESM1 buoyancy-driven SST anomaly field from 90°S-11°S and 11°N-90°N.
 276 We linearly taper this forcing to zero over 5° to 6°S and 6°N to avoid artificially large
 277 meridional forcing gradients. There is no anomalous SST forcing from 5°S-5°N in the
 278 extratropical SST forcing experiment. Similarly, in the equatorial SST forcing experi-
 279 ment we apply the full CESM1 buoyancy-driven SST anomaly field from 5°S-5°N, cre-
 280 ate a 5° linear taper to 10°S and 10°N, and do not anomalously force SST anywhere else.
 281 While we somewhat arbitrarily chose these meridional boundaries, we have found that
 282 using 10°S and 10°N for the full forcing bounds of the equatorial SST forced simulation
 283 (and changing other bounds accordingly) leads to small differences that do not affect our
 284 conclusions (not shown). Last, as a point of comparison with the extratropical SST forc-
 285 ing simulation described above, we consider the NEPac2CWarm simulation originally
 286 presented in Luongo et al. (2025), where a rectangular patch of +2°C SST warming is
 287 applied off the coast of California. For all OGCM simulations we consider the average
 288 over years 11-30 after the forcing is applied as in Luongo et al. (2025).

289 **2.4 Reduced Gravity Simulations**

290 Finally, we run two simulations using the 1.5-layer reduced gravity (RG) model to
 291 represent an idealization of the upper ocean’s response to an increase in surface strat-
 292 ification. The set-up is borrowed directly from Sun and Thompson (2020), with geog-
 293 raphy consisting of three idealized ocean basins representing the Atlantic, Indian, and
 294 Pacific oceans and a zonally re-entrant channel representing the Southern Ocean from
 295 45°S to the southern boundary. The total width is 220° and the latitudinal extent is from
 296 72°S-72°N. The model solves for upper layer thickness, approximating thermocline depth,
 297 and has a 1° horizontal spacing. Sun and Thompson (2020) provide further details on
 298 this model.

299 We run two reduced gravity simulations. The first is a control simulation using stan-
 300 dard parameters from Sun and Thompson (2020) (RGCtrl). The second branches from
 301 the tenth year of RGCtrl and instantaneously doubles the reduced gravity parameter to
 302 represent a stratification increase in response to climate change forcing (RGx2). We com-
 303 pare the difference between these two simulations ten years after that branch point.

3 Results

3.1 Buoyancy and Momentum Dynamics Create the Full Response

Despite the fact that our CESM1 simulations idealize climate change as an abrupt quadrupling of CO₂, the upper-ocean quasi-steady fully-coupled (FC) response (Figure 2a) bears a striking resemblance to the multi-ensemble mean response to realistic historical forcing in Figure 1b (Pearson pattern correlation of 0.94). As in the multi-model response, the FC equatorial temperature response features a thermocline cooling in the central Pacific, a strong surface warming that is deeper in the western Pacific than the eastern Pacific, and a sub-thermocline warming in the eastern Pacific. Luo et al. (2018) show a very similar CESM1 response to abrupt quadrupling of CO₂ (over years 41-90), which in turn also resembles the transient response (years 1-10) to this same forcing in two prior versions of CESM (Heede et al., 2021). It is interesting that the equatorial Pacific’s subsurface temperature response to abrupt idealized climate change matches the response pattern to historical forcing so well, particularly since Heede et al. (2021) showed that the prominent thermocline cooling response to abrupt quadrupling disappears after 200 years and is instead replaced by a near-zero temperature response. While the centennial response to abrupt 4xCO₂ forcing is an unrealistic analog for transient climate change, the multi-decadal response to abrupt 4xCO₂ forcing shown in Figure 2a appears to be an appropriate tool for studying the multi-model response to greenhouse warming.

As in Luongo et al. (2023), who instead consider the subsurface equatorial temperature response to NH ETINMIP forcing, we find that the FC equatorial temperature response to CO₂ forcing (Figure 2a) is highly linear. That is, the fully-coupled (FC) response to CO₂ forcing can be neatly linearly decomposed into the buoyancy-forced (BF) response (Figure 2b) and the momentum-forced (MF) response (Figure 2c):

$$FC \approx BF + MF . \tag{1}$$

Comparing Figure 2a with the sum of Figures 2b & c explicitly shows this linearity (Figure S3a). These patterns closely resemble the FC, BF, and MF responses to NH ETINMIP forcing (but with opposite sign because ETINMIP forcing is a cooling) presented in Luongo et al. (2023) and recreated in Figures S4a-c. This resemblance is also found

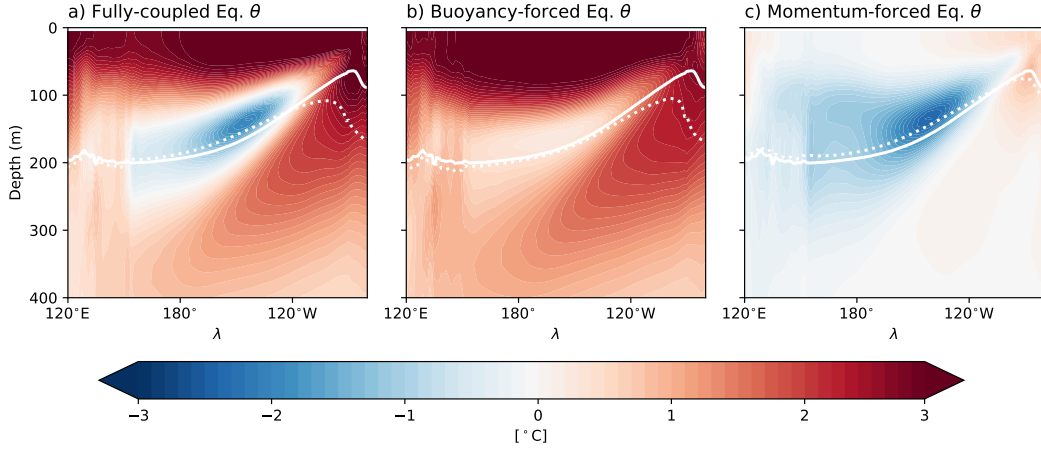


Figure 2. a) CESM1 fully-coupled (FC = CO₂x4-Ctrl) equatorial temperature (θ) response to abrupt quadrupling of CO₂. b) CESM1 buoyancy-forced (BF = Tau1CO₂x4-Tau1CO₂x1) equatorial θ response to abrupt quadrupling of CO₂. c) CESM1 momentum-forced (MF = Tau4CO₂x1-Tau1CO₂x1) equatorial θ response to abrupt quadrupling of CO₂. All panels are meridionally averaged from 5°S-5°N and temporally averaged from years 11-50. The 16°C isotherm from Ctrl is plotted as a solid white contour in all three panels and approximates the mean thermocline. Dotted white contours are the 16°C isotherm in the forced experiments: a) CO₂x4, b) Tau1CO₂x4, and c) Tau4CO₂x1.

333 in response to SH ETINMIP forcing (Figure S4d-f). This similarity between equatorial
 334 temperature responses was not expected a priori because abrupt 4xCO₂ is a nearly hemi-
 335 spherically symmetric forcing while ETINMIP forcing is purposefully hemispherically
 336 asymmetric. We discuss this further in Section 4.

337 The MF response, created by momentum-driven dynamics, is the cause of the promi-
 338 nent thermocline cooling seen in the FC response, qualitatively agreeing with Jiang et
 339 al. (2024b, 2025)'s assertion that winds have driven much of the observed subsurface equa-
 340 torial temperature response. This cooling is maximized within the thermocline and is
 341 a major feature across the majority of the basin. However, while weak cooling extends
 342 from surface to depth in the western Pacific, even the strong cooling in the thermocline
 343 dissipates before reaching the eastern boundary. Instead the eastern equatorial Pacific
 344 from the surface to below the thermocline features weak warming. This zonal temper-
 345 ature dipole is a feature of relaxed thermocline tilt: a shoaling of the western Pacific ther-
 346 mocline and a deepening of the eastern Pacific thermocline would respectively manifest

347 as a cooling and warming in depth space. The relaxed thermocline tilt in FC, partially
348 caused by strong westerly anomalies in equatorial wind stress (Figure S5c), partially agrees
349 with Vecchi and Soden (2007)'s hypothesis that the thermocline cooling response to cli-
350 mate change results from a decadal Bjerknes-like response to relaxed wind stress. Ad-
351 ditionally, slightly weakened STCs in our MF experiment (not shown) could contribute
352 to this cooling as well (Yang et al., 2009; Jiang et al., 2025). While both dynamics, re-
353 duced thermocline tilt and reduced STC strength, likely contribute to the MF cooling,
354 we hesitate to say whether one is more or less likely to have occurred over 1958-2020 due
355 to disagreement between reanalysis-estimated wind stress that could hypothetically sup-
356 port either mechanism (Figure S5). We do note, however, that because the MF response
357 does not include greenhouse-gas-driven increases in subtropical stratification, and yet
358 it accounts for all FC thermocline cooling, that this understanding disagrees with the
359 arguments proposed by Luo et al. (2009, 2018) and Ju et al. (2022) that increased sub-
360 tropical stratification creates this cooling by either slowing the STCs or advecting density-
361 compensated anomalies.

362 Perhaps unsurprisingly, the BF response, which captures the ocean's response to
363 anomalous buoyancy fluxes from increased CO₂ radiative forcing, contributes nearly all
364 of the warming seen in FC. This includes a strong surface warming maximized in the cen-
365 tral Pacific and most of the eastern Pacific's sub-thermocline warming. Interestingly, the
366 central Pacific thermocline region in BF has a near-zero temperature response in the ex-
367 act same region where MF cools. This allows the relatively strong momentum-driven cool-
368 ing to clearly establish itself in FC. The near-zero temperature response of the BF ther-
369 mocline, which strongly resembles the full centennial response to abrupt CO₂ quadru-
370 pling seen in Heede et al. (2021), also implies a relatively long-lasting upwelling damp-
371 ing effect.

372 This BF pattern, with its near-zero thermocline response, strong surface warming,
373 and sloping sub-thermocline eastern Pacific warming, is not obviously attributable to well-
374 known dynamics. Both conventional advective (ocean-tunnel) and dynamical (wave-driven)
375 understandings of the STCs instead suggest broad thermocline warming. While Luongo
376 et al. (2023) perform an ocean mixed layer heat decomposition on the equatorial SST
377 response to NH ETINMIP forcing and attribute a certain amount of the BF SST response
378 to ocean dynamics, the specific dynamic adjustments remain unclear. As such, we turn

379 to MITgcm ocean-only simulations to explain the ocean dynamics that create the sub-
 380 surface BF response to climate change forcing seen in Figure 2b.

381 **3.2 Recreating the Buoyancy Response**

382 To determine whether MITgcm is an appropriate tool with which to understand
 383 the ocean dynamics that create the buoyancy-driven mechanically-decoupled CESM1’s
 384 response in Figure 2b, we first test whether MITgcm is able to effectively recreate CESM1’s
 385 response at all. In the CO₂x4_BFsst OGCM simulation we add the global quasi-steady
 386 buoyancy-forced SST response to abrupt 4xCO₂ forcing (Figure 3a) to MITgcm’s monthly
 387 climatological SST relaxation fields. Because we do not change any other forcing fields,
 388 the difference between this simulation and OCtrl is the ocean-only response to that SST
 389 forcing pattern.

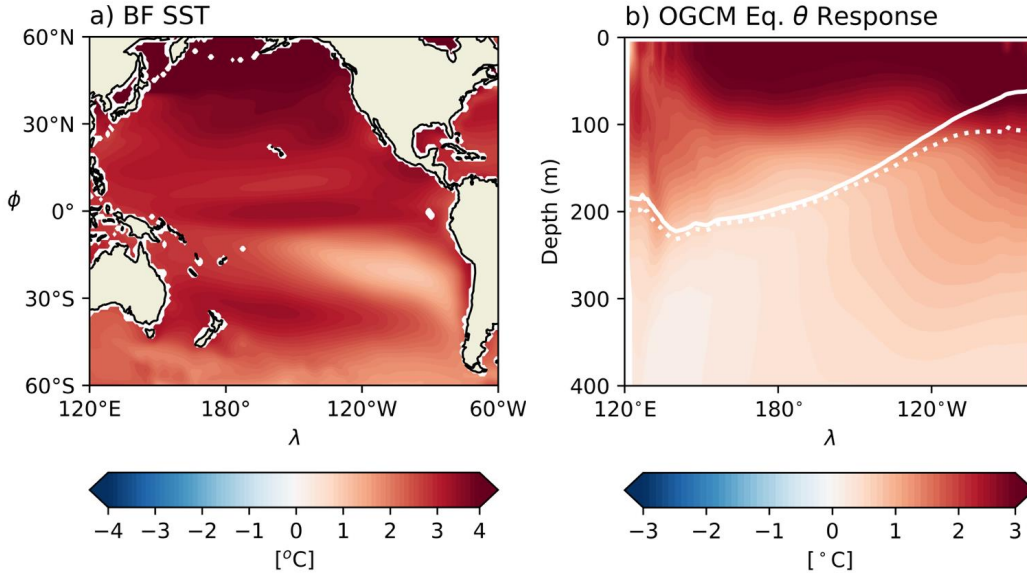


Figure 3. a) Buoyancy-forced quasi-steady (year 11-50) SST response in CESM1. b) MITgcm equatorial temperature (θ) response to BF SST forcing in panel a) averaged over years 11-30: CO₂x4_BFsst-OCtrl. The 16°C isotherm in OCtrl (solid white contour) approximates the mean thermocline and the 16°C isotherm in CO₂x4_BFsst (dotted white contour) approximates the forced thermocline.

390 MITgcm does a surprisingly good job of recreating the major features of CESM1’s
 391 quasi-steady buoyancy-forced subsurface equatorial temperature response (c.f. Figures

392 2b and 3b, Pearson pattern correlation of 0.86). The MITgcm temperature response fea-
393 tures the strong, relatively zonally symmetric near-surface warming, a warming mini-
394 mum in the central-western Pacific thermocline, and sloping sub-thermocline warming
395 in the eastern Pacific. There are some notable differences between the two patterns, most
396 obviously that the near-zero thermocline warming so obvious in CESM1 is deeper, more
397 westward, and more diffuse in MITgcm. The eastern Pacific sub-thermocline warming
398 is also weaker in MITgcm. However, MITgcm and CESM1's ocean component are dif-
399 ferent models with differences in mean state, parameterizations, and resolution. Given
400 this reality, we consider the otherwise substantial agreement between Figures 2b and 3b
401 to be promising, and we conclude that these ocean-only simulations are a reasonable di-
402 agnostic tool for understanding mechanically-decoupled simulations.

403 Having shown that the MITgcm response to the full BF SST field reasonably recre-
404 ates the CESM1 response, we now ask whether we can decompose this full response fur-
405 ther, namely into the response to SST forcing from different geographic regions. This
406 question emerges directly from the canonical advective ocean tunnel understanding of
407 the non-wind-driven STC response to climate change (e.g., Clement et al., 1996; Luo et
408 al., 2009, 2017, 2018; Heede & Fedorov, 2021; Ju et al., 2022), which suggests that warm
409 subtropical surface waters subduct in the eastern half of the subtropical gyre, are car-
410 ried by mean advection to the western boundary, penetrate into the tropics via low lat-
411 itude western boundary currents, and eventually warm the thermocline. Because this
412 understanding suggests that some portion of the equatorial temperature response is en-
413 tirely remotely-driven, we run two OGCM simulations to determine whether we can un-
414 derstand the full response to BF SST forcing as the sum of patterns created by remote
415 and local SST forcing. We do this by regionally partitioning the full BF SST forcing field
416 in Figure 3a into remote extratropical (ET: Figure 4a) and local equatorial (EQ: Fig-
417 ure 4b) SST forcing fields.

418 The sum of the remote (Figure 4c) and local (Figure 4d) responses almost perfectly
419 recreates the full field response in Figure 3b (Figure S3b, Pearson pattern correlation of
420 0.98). However, while these patterns sum to the full response, they differ substantially
421 and clearly represent different oceanic dynamics. We explore the ocean adjustments that
422 create the remote and local response in the following two subsections.

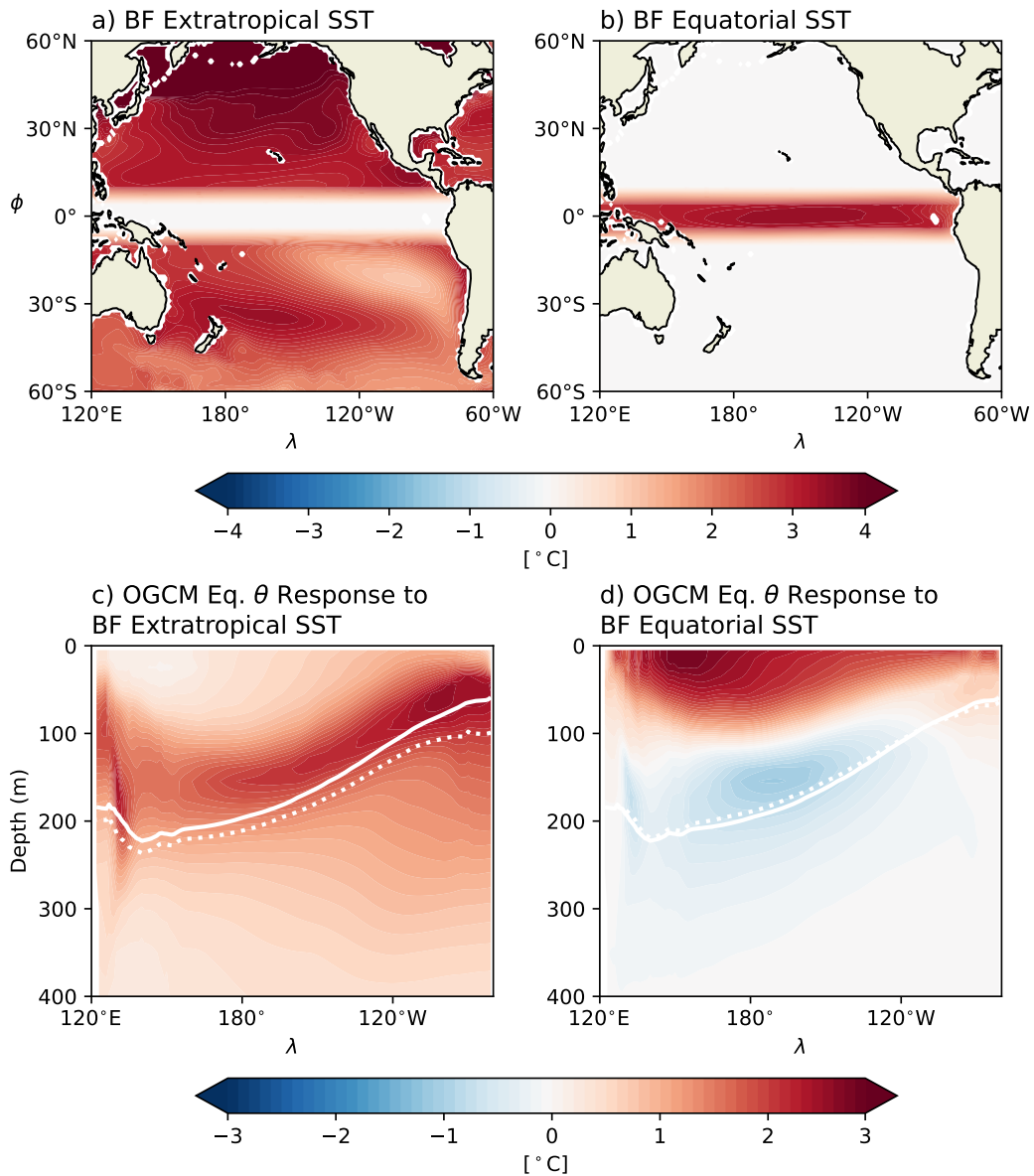


Figure 4. a) Remote, extratropical component of BF SST response in Figure 3a. b) Local, equatorial component of BF SST response in Figure 3a. c) Equatorial temperature (θ) response to remote SST forcing in panel a): CO₂x4.BFsstET-OCtrl. d) Equatorial θ response to local SST forcing in panel b): CO₂x4.BFsstEQ-OCtrl. The 16°C isotherm in OCtrl (solid white contour in panels c & d) approximates the mean thermocline and the 16°C isotherm in CO₂x4.BFsstET and CO₂x4.BFsstEQ (dotted white contours in panels c & d, respectively) approximates the perturbed thermocline.

423 **3.2.1 Adjustments to Remote Buoyancy Forcing**

424 We first consider the equatorial temperature response to extratropical-only BF SST
 425 forcing (Figure 4c). The equatorial Pacific subsurface warms in response to this remote
 426 forcing, with no evidence of cooling. The warming is maximized within the thermocline
 427 throughout the entire basin. Despite strong surface relaxation to unperturbed SSTs, the
 428 strong near-surface thermocline warming in the eastern equatorial Pacific extends to the
 429 surface. In addition, it is clear that the sloping sub-thermocline warming in the eastern
 430 Pacific noted in the FC and BF CESM1 responses above is caused by this remote ad-
 431 justment.

432 This coherent warming of the equatorial thermocline in response to remote SST
 433 forcing in both hemispheres is strikingly similar to the equatorial temperature response
 434 to a +2°C SST anomaly in the northeast Pacific stratocumulus deck as presented in Luongo
 435 et al. (2025)’s NEPac2CWarm simulation (c.f. Figures 4c and 5b, Pearson pattern cor-
 436 relation of 0.94). In that study we used MITgcm to investigate how the tropical ocean
 437 responded to subtropical surface cooling. We showed that both circulation adjustments
 438 driven by baroclinic planetary waves ($v'\bar{\theta}$) and mean advection of temperature anoma-
 439 lies within the subtropical gyre and low latitude western boundary currents ($\bar{v}\theta'$) com-
 440 municated subtropical cooling to the tropics within about a decade. At the equator, an
 441 equatorial Kelvin wave coherently heaved the thermocline as it traveled eastward. Upon
 442 hitting the eastern boundary, this wave signal radiated poleward in both hemispheres
 443 as coastal Kelvin waves, which then proceed to adjust stratification in the eastern basin
 444 by shedding westward-propagating Rossby waves. Although we primarily focused on sub-
 445 tropical cooling in Luongo et al. (2025), the NEPac2CWarm response presented in Fig-
 446 ure 5 demonstrates that the equatorial temperature response to subtropical warming is
 447 simply the opposite of its response to subtropical cooling. It is also relevant to note that
 448 Luongo et al. (2025) showed that both NH and SH subtropical forcing led to similar equa-
 449 torial response patterns due to the symmetric nature of the equatorial Kelvin wave ad-
 450 justment.

451 In the case of CO₂x4_BFsstET, the dynamics clarified in Luongo et al. (2025) sug-
 452 gest that strong subtropical warming present in both NH and SH (Figure 4a) contribute
 453 to the warming of the equatorial thermocline (Figure 4c). This warming occurs through
 454 both mean advection of warm anomalies, as in the canonical ocean tunnel understand-

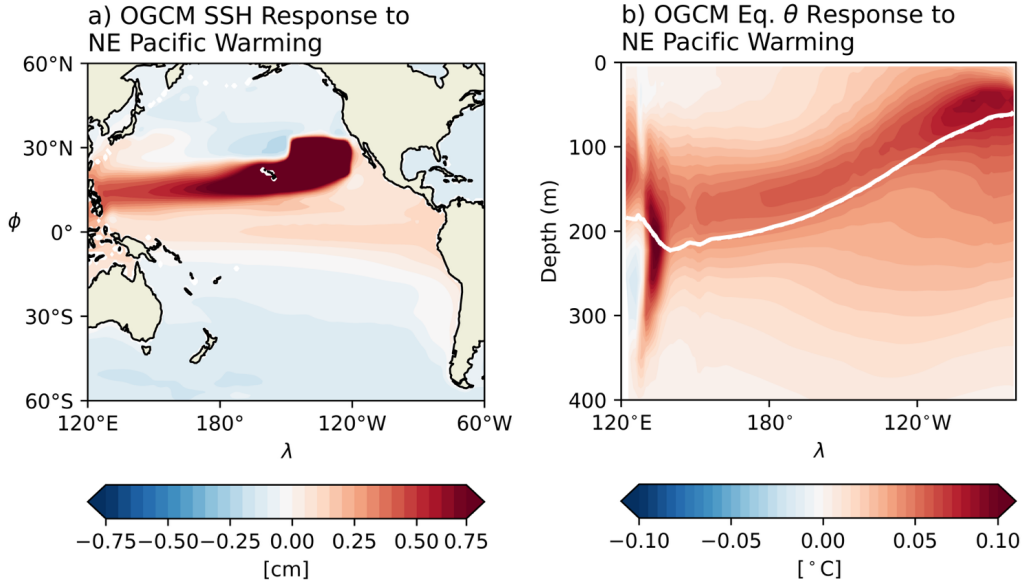


Figure 5. a) Sea surface height (SSH) response (NEPac2CWarm-OCtrl) to Northeast Pacific warming patch from Luongo et al. (2025). b) Equatorial temperature (θ) response to NEPac2CWarm simulation. The 16°C isotherm in OCtrl (solid white contour) approximates the mean thermocline and the 16°C isotherm in NEPac2CWarm (dotted white contour) approximates the forced thermocline.

455 ing, but also due to the coherent deepening of the equatorial thermocline via a down-
 456 welling Kelvin wave excited by the subtropical gyres' baroclinic response to anomalous
 457 surface warming. This dynamical adjustment is in-turn responsible for the eastern Pa-
 458 cific's sloping sub-thermocline warming, a slow stratification adjustment to the heaved
 459 thermocline. As such, while the difference in magnitude between Figures 4c and 5b re-
 460 sults from the much stronger forcing from CO_2 quadrupling in $\text{CO}_2 \times 4$.BFsstET com-
 461 pared to the relatively small patch of $+2^{\circ}\text{C}$ warming in NEPac2CWarm, the strong sim-
 462 ilarity in pattern re-emphasizes the importance of the STC as a dynamic mechanism to
 463 communicate subtropical warming to the equatorial thermocline.

464 **3.2.2 Adjustments to Local Buoyancy Forcing**

465 The response of the subsurface equatorial Pacific to the local buoyancy-forced com-
 466 ponent of climate change forcing (Figure 4d) unsurprisingly features strong near-surface
 467 warming which is directly tied to the applied tropical SST forcing (Figure 4b). However,

perhaps unexpectedly, the local response features substantial cooling across much of the thermocline that underlies the strong near-surface warming. In the western Pacific, where the mean thermocline and anomalous near-surface warming signal are deepest, this thermocline cooling response extends from approximately 100-400m. As the mean thermocline tilts upward to the east, this cooling signal gets shallower and thinner until the temperature anomaly switches signs to warming around 110°W. The thermocline then remains anomalously warm all the way to the eastern boundary.

Luo et al. (2018) used an OGCM to explore the response of the equatorial thermocline to a uniform tropical warming of 3.2°C. They find a pattern of near-surface warming and thermocline cooling that is similar to our response to local BF. In that work, Luo et al. (2018) suggested that this temperature response was a local baroclinic adjustment to surface warming: as near-surface stratification increases in response to surface warming, turbulent downward mixing of that heat decreases and creates a cooling signal (Yang et al., 2009). Luo et al. (2018), therefore, would attribute much of the cooling in Figure 4d to be a signal of reduced mixing. We note, however, that this mechanism does not explain the zonal temperature dipole clearly seen in our thermocline response to local BF: as discussed above, a zonal dipole instead implies a thermocline tilt and suggests the need to consider zonal gradients.

To determine whether the local response can instead be understood in terms of inviscid dynamics, we model the equatorial ocean as a simple 1.5-layer reduced gravity system. In this simplified understanding, the lower level flow is negligible compared to upper level flow ($\vec{u}_1, \vec{v}_1 \gg \vec{u}_2, \vec{v}_2 = 0$), the layers are coupled by their density differences via the reduced gravity parameter [$g' \equiv g(\rho_2 - \rho_1)/\rho_2$], and the interface depth, $h = \eta + H$, is thermocline depth defined positive downward and as a sum of interface displacement η and mean thermocline depth H . Ignoring dissipation terms, the steady, linear equatorial zonal momentum equation in conservative flux form is

$$0 = -\left(g' \frac{h^2}{2}\right)_x + \frac{\tau^x}{\rho_0}, \quad (2)$$

where τ^x is zonal wind stress, ρ_0 is a constant reference density, and the x subscript represents a zonal derivative. If we now instead consider the non-conservative velocity form of Equation 2 linearized about H ,

$$0 = -g' \eta_x + \frac{\tau^x}{\rho_0 H}, \quad (3)$$

497 and we consider a uniform Δ climate change forcing without changes in τ^x (as is the case
 498 in our OGCM simulations), the balance becomes

$$\Delta g' \overline{\eta_x} = -\overline{g'} \Delta \eta_x. \quad (4)$$

499 Equation 4 demonstrates, without making any assumptions about the eastern bound-
 500 ary, that the product of the perturbed RG and the mean zonal gradient of interface dis-
 501 placement must be balanced by the product of the mean RG and a perturbed zonal gra-
 502 dient of interface displacement. In the case of climate change driven warming, because
 503 $\Delta g' > 0$ we expect $\Delta \eta_x > 0$. Put another way, an increase in stratification should re-
 504 duce the tilt of the thermocline even with no change in winds, in turn leading to west-
 505 ern thermocline cooling and eastern thermocline warming.

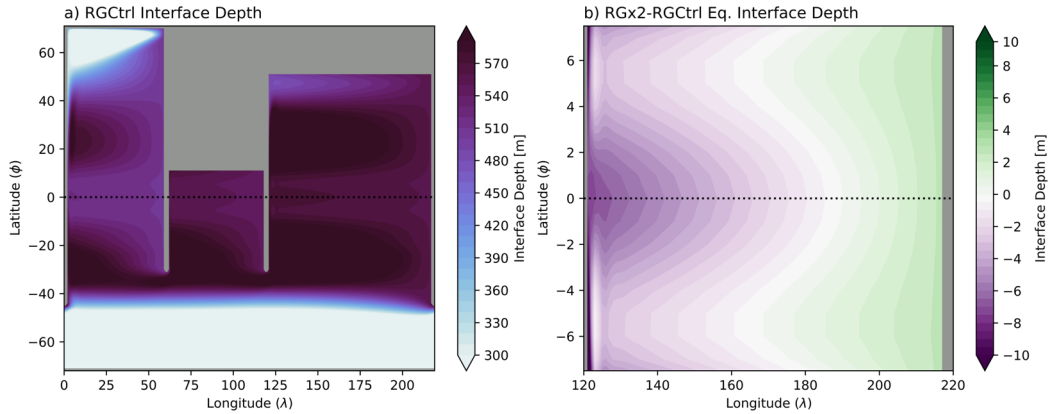


Figure 6. a) Interface depth in idealized global RG model after 20 years of spin-up in RGC-
 ctrl. b) Equatorial interface depth response to RGx2-RGCtrl’s doubling of reduced gravity at year
 10.

506 We test this tilt hypothesis with two simulations using Sun and Thompson (2020)’s
 507 idealized global ocean reduced gravity model (Figure 6a), comparing a simulation where
 508 the reduced gravity parameter is doubled (RGx2) to one where it isn’t (RGCtrl). While
 509 a doubling of stratification is a relatively large forcing, it is on the same order as the near-
 510 surface equatorial Pacific increase in stratification observed in the BF response (not shown).
 511 Figure 6b shows the η response in the equatorial Pacific 10 years after RG is doubled.

512 We see that the western equatorial Pacific interface displacement decreases (shoals), while
 513 the eastern equatorial Pacific interface displacement increases (deepens). This western
 514 Pacific shoaling and eastern Pacific deepening corresponds to a relaxation in thermocline
 515 tilt, or a western thermocline cooling and an eastern thermocline warming. We use this
 516 newly gained physical intuition to explain the thermocline temperature dipole in Fig-
 517 ure 4d, which then adds to the coherent thermocline shoaling pointed out by Luo et al.
 518 (2018).

519 In summary, we conclude that the local response of the equatorial thermocline to
 520 the equatorial buoyancy-driven SST response to climate change consists of two responses
 521 to the increase in near-surface stratification: both a coherent thermocline shoaling and
 522 a decrease in thermocline tilt. This latter point questions the oft-held view that a tilted
 523 thermocline is necessarily tied to a change in zonal winds.

524 4 Discussion

525 4.1 Linearity of the Equatorial Thermocline’s Response

526 We use a hierarchy of models to show that the full subsurface temperature response
 527 of the equatorial thermocline to greenhouse gas forcing (θ_{FC} : Figure 2a) can be recov-
 528 ered as a relatively simple linear combination of independent ocean dynamical responses.
 529 As in Luongo et al. (2023), we use a mechanically decoupled model to show that θ_{FC}
 530 is the sum of the wind stress-driven response (θ_{MF} : Figure 2c) and the buoyancy-driven
 531 response (θ_{BF} : Figure 2b). We then use OGCM simulations to show that θ_{BF} can be
 532 linearly partitioned into a sum of forced responses from different geographic regions of
 533 SST forcing: a remote, extratropically-driven response ($\theta_{BF,remote}$: Figure 4c) and a lo-
 534 cal, equatorially-driven response ($\theta_{BF,local}$: Figure 4d). The remote response represents
 535 the dynamically and thermodynamically-driven changes of the thermocline in response
 536 to subtropical temperature forcing, as outlined in Luongo et al. (2025). We then use a
 537 RG model to show that the local response is consistent with a response to surface strat-
 538 ification that includes both shoaling and reduced thermocline tilt. Putting this all to-
 539 gether, we present this linear understanding as

$$\begin{aligned} \theta_{FC} &= \theta_{MF} + \theta_{BF} = \theta_{MF} + \theta_{BF,remote} + \theta_{BF,local} \\ &= \alpha * MF(\tau^x, \tau^y) + \beta * BF_{remote}(NH\ SST, SH\ SST) + \gamma * BF_{local}(Eq.\ SST) . \end{aligned} \quad (5)$$

Equation 5 communicates that the full response of the modeled tropical Pacific subsurface temperature response to greenhouse gas forcing is a linear combination of ocean dynamics driven by momentum from zonal and meridional wind stress, buoyancy from NH and SH subtropical SST forcing, and buoyancy from local equatorial SST forcing, with α , β , and γ as scaling coefficients. This is the primary result of our study. Because our FC CESM1 response to abrupt quadrupling of CO₂ strongly resembles both the 1958-2020 observed (Figure 1a) and multi-model mean (Figure 1b) response to realistic, historical climate change forcing, we conclude that this simple linear understanding gained from a hierarchy of idealized modeling simulations is a powerfully relevant and applicable tool with which to understand realistic climate change.

While this understanding is simple at face value, it in fact suggests that the equatorial temperature response to even just steady, idealized greenhouse gas forcing is more complex than previously understood. We see that the full response actually contains many of the dynamics previously suggested in the literature (e.g. Clement et al., 1996; Seager & Murtugudde, 1997; Vecchi & Soden, 2007; Luo et al., 2009, 2018; Heede et al., 2020, 2021; Watanabe et al., 2024). Nevertheless, it is only through understanding the combination of these dynamics that we can critically update our theoretical picture for how the equatorial Pacific will respond to climate change.

4.2 Reconstructing Long and Short-Term Climate Change Responses

As suggested by Equation 5, we seek to reconstruct the observed equatorial subsurface temperature trends from 1958-2020 (Figure 1a) as a linear combination of the MF and remote and local BF patterns. We use a depth-weighted ordinary least squares multilinear regression to determine combination coefficients. Our reconstruction of the 1958-2020 trend (Figure 7a) shows strong agreement with the observational composite (Figure 1a), with a Pearson pattern correlation of 0.86. We are able to explain much of both the models' and observations' long-term subsurface temperature response through our linear understanding of oceanic dynamics. Interestingly, we note that while the regression coefficients for the MF and local BF responses are positive (meaning they are in line with positive greenhouse gas forcing), the remote BF response is slightly negative (Figure 7c). This suggests that subtropical temperature forcing has not majorly impacted the equatorial thermocline in this period, and, if it has, it's been a cooling signal. This could hypothetically be due to a communication of the observed subtropical

572 Southeast Pacific surface cooling (Wills et al., 2022) via the subtropical cells (Luongo
573 et al., 2025).

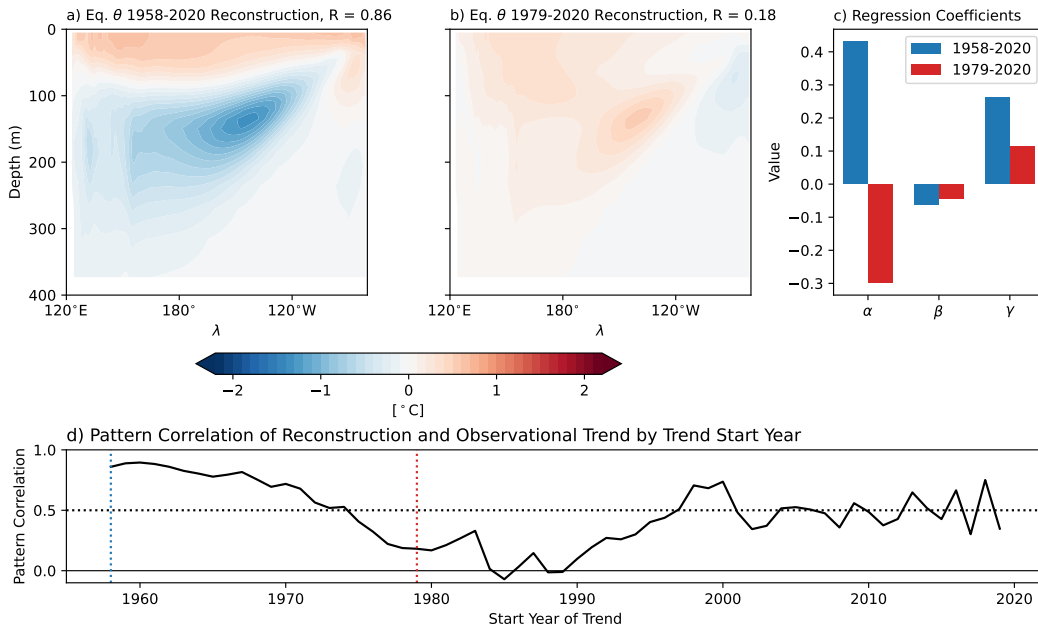


Figure 7. a) 1958-2020 reconstruction of Figure 1a observational trend using α *MF pattern + β *remote BF pattern + γ *local BF pattern as in Equation 5. b) As in a), but for 1979-2020 observational trend of Figure 1c. c) Regression coefficients for linear combinations in a) and b). d) Pearson pattern correlation between regression-estimated reconstruction and observed trend as a function of trend start year. The dotted blue line highlights 1958, the dotted red line highlights 1979, and the dotted black line is at a correlation value of 0.5.

574 While the multi-model mean trend is obviously similar to the observed trend over
575 1958-2020, the observed 1979-2020 trend is notably distinct from the modeled trend over
576 that same period (c.f. Figure 1c & d). Indeed, our multilinear regression method can not
577 successfully reconstruct this more recent period's observed temperature trend (Figure
578 7b, Pearson correlation 0.18). In fact, the regression coefficients suggest that the best
579 way to reconstruct the strong subsurface western Pacific warming in the 1979-2020 trend
580 is via a momentum-forced response opposite to that caused by CO₂ forcing (Figure 7c).
581 Although the understanding gained in Equation 5 works for longer-term temperature trends,
582 it breaks down for the more recent past.

583 The disagreement between models' and observations' SST trends over this period
584 has been the focus of many recent studies (e.g., Wills et al., 2022; Watanabe et al., 2024);
585 our result underlines this disagreement further. We highlight two implications of this re-
586 sult. First, while Seager et al. (2019) and Jiang et al. (2025) emphasize how differences
587 between observations and model mean states could impact SSTs, and although GCM
588 mean states are certainly biased, the GCMs are clearly able to recreate the longer-term
589 subsurface temperature response to historical forcing, as long as the trend starts before
590 ~ 1975 (Figure 1e). This conclusion, combined with recent results from Dhame et al. (2025),
591 who showed that while higher resolution simulations reduce mean state biases they do
592 not necessarily simulate temperature trends better, suggests that mean state biases are
593 not the only cause of disagreement in trends over the past 40 years. This suggests that
594 despite equatorial mean state biases our climate models are not hopelessly unfit for the
595 task of climate change projections.

596 Second, this result suggests an important role for internal variability in recent equa-
597 torial Pacific thermocline temperature trends: we simply cannot recreate the observed
598 pattern of subsurface temperature since the late 1970s with our linear understanding of
599 the ocean's response to different quasi-steady forcings. Even making the MF coefficient
600 negative, consistent with an observed strengthening Walker circulation (L'Heureux et
601 al., 2013), is not enough to recreate the observed dipole in the equatorial thermocline.
602 Because our patterns are quasi-steady, internal variability is an obvious culprit. Figure
603 7d shows how the pattern correlation between our regression-estimated reconstruction
604 and observational trend changes as a function of start year of the trend. Trends which
605 start before 1975 are skillfully reconstructed from our linear understanding, presumably
606 because enough cycles of internal variability have been averaged out to clarify the re-
607 sponse. The linear reconstruction specifically fails, however, when attempting to recon-
608 struct trends that begin between 1975-2000, a period when models and observations dis-
609 agree the most (Figure 1e) and which also happens to coincide with several strong El
610 Niño events.

611 Nevertheless, we can definitively say the dynamics we have emphasized here, decadal
612 momentum-driven thermocline tilt, subtropical cell adjustment, and equatorial stratification-
613 induced thermocline shoaling and tilt, contribute less to the 1979-2020 trend than has
614 been commonly hypothesized [e.g., Figure 4 schematic of Watanabe et al. (2024)]. We
615 hypothesize that recent internally-driven climate variability, such as ENSO or tropical

616 Pacific decadal variability (Capotondi et al., 2023), which is not included in our pattern
 617 reconstructions, has critically crafted observed subsurface equatorial Pacific temperature
 618 trends over the past 40 years. This conclusion is in line with Jiang et al. (2024a), who
 619 emphasize the role of the Interdecadal Pacific Oscillation on SST patterns over that same
 620 period.

621 **4.3 Implications for the Canonical Ocean Dynamical Thermostat**

622 The simplicity of this linear understanding allows us to interrogate the canonical
 623 view of the ocean-tunnel-mediated ocean dynamical thermostat as a mechanism for un-
 624 derstanding recent equatorial Pacific climate change. In this view, which largely rests
 625 on a mean advective understanding of the STCs ($\bar{v}\theta'$), anomalous subtropical warming
 626 is communicated to the equatorial thermocline after some lag to erode the relative cool-
 627 ing initially created by continued mean upwelling of unperturbed waters. As such, the
 628 conventional view of the ocean dynamical thermostat mechanism has been limited to a
 629 transient phenomenon. This understanding has been used to suggest that while the trop-
 630 ical Pacific's response to climate change may start as La Niña-like, as in recent obser-
 631 vations, it will eventually transition to El Niño-like as suggested by the vast majority
 632 of model projections (Heede et al., 2020, 2021; Watanabe et al., 2024).

633 Our remote, buoyancy-driven response indeed shows that subtropical SST warm-
 634 ing in the extratropics coherently warms the thermocline. While Luongo et al. (2025)
 635 show that this pattern is best understood as having been created by wave dynamics, the
 636 basic understanding that subtropical SSTs warm the equatorial thermocline via the STCs
 637 holds true. In the framework of the upwelling damping effect of mean vertical advection
 638 on equatorial SSTs ($-\bar{w}\theta'_z \equiv -\bar{w}\frac{\theta'_s - \theta'_e}{H_e}$; e.g., Xie et al., 2010), where the s and e sub-
 639 scripts are respectively surface and entrainment levels and H_e is the depth of the entrain-
 640 ment level to the surface, initially $\theta'_e < \theta'_s$ and so mean upwelling cools, but eventually
 641 $\theta'_e > \theta'_s$ and mean upwelling warms.

642 However, our remote and local MITgcm simulations show that this is a delicate bal-
 643 ance: the remotely-driven thermocline warming (Figure 4c) is entirely canceled out (Fig-
 644 ure 2b & 3b) by the locally-driven thermocline cooling (Figure 4d). In the case of our
 645 simulations, subtropical warming only works to erode the local cooling from thermocline
 646 shoaling and decreased thermocline tilt such that the final, steady thermocline temper-
 647 ature response is near-zero ($\theta'_e \approx 0$) and there is no sign change in $-\bar{w}\theta'_z$ with time. This

648 implies a long-lasting upwelling damping effect. Our model simulations, therefore, sug-
649 gest that the canonical view of the thermostat necessarily leading to a transient response
650 (as has been used to explain recent observations) is misleading. Rather, we emphasize
651 that the relative ratio of tropically-driven cooling to extratropically-driven warming is
652 critical to understand timescales associated with the buoyancy-driven response. In our
653 case, which in turn resembles the near-steady, centennial response to abrupt quadrupling
654 of CO₂ (Heede et al., 2021), remote warming simply cancels out local cooling such that
655 there is no major warming of the thermocline from SST forcing at all (Figures 2b & 3b).
656 If instead, however, the extratropically-driven warming was much larger than the tropically-
657 driven cooling we might expect a correlation between subtropical to tropical meridional
658 SST gradients and the tropical zonal SST gradient (Burls & Fedorov, 2014).

659 **4.4 Symmetry of Equatorial Responses**

660 A final surprising detail of this study is the immutability of the equatorial Pacific
661 subsurface temperature response regardless of forcing geography. This is best seen by
662 comparing the FC, BF, and MF responses to abrupt quadrupling of CO₂ (Figure 2) to
663 those same responses to NH and SH ETINMIP forcing (Figure S4). Despite the fact that
664 CO₂ forcing is primarily equatorially symmetric and ETINMIP forcing is purposefully
665 equatorially asymmetric, the response patterns are effectively the same (with an oppo-
666 site sign). From the perspective of the equatorial Pacific subsurface, it would be diffi-
667 cult to immediately tell the difference between greenhouse gas warming and a hypothet-
668 ical extratropical warming (e.g., Tseng et al., 2023). This similarity extends to the lin-
669 ear partitioning of the buoyancy-driven response into remote and local forcing (Figure
670 S6). The equatorially symmetric nature of the equatorial thermocline’s response to sub-
671 tropical forcing (Luongo et al., 2025) creates the same remote response pattern as if both
672 hemispheres’ subtropics were forced. Because the local response just depends on an in-
673 crease or decrease in surface stratification, the equatorial response to local forcing looks
674 effectively the same.

675 This understanding raises two interesting points. First, it highlights that hemispheric
676 asymmetries in meridional forcing, crucial to the zonal-mean energetic framework through
677 which we understand ITCZ shifts (Kang et al., 2008) and cross-equatorial ocean heat
678 transport (Luongo et al., 2022), do not lead to appreciably different equatorial temper-
679 ature responses. Despite the fact that ETINMIP forcing drives strong cross-equatorial

680 responses, the equatorial thermocline simply cares if the forcing causes large-scale warm-
681 ing or cooling. Second, the equatorial thermocline’s response to industrial aerosol forc-
682 ing (similar to NH ETINMIP forcing) would not lead to an independent temperature
683 pattern from greenhouse gas forcing. Put another way, NH aerosol forcing would sim-
684 ply modulate the tropical Pacific’s response to greenhouse gas forcing rather than cre-
685 ate a fundamentally different pattern.

686 5 Conclusions

687 In this study we have used a series of climate modeling simulations of varied com-
688 plexity to understand the equatorial thermocline response to climate change. We first
689 show that a multi-model mean of 11 large ensembles reasonably captures the observed
690 1958-2020 subsurface equatorial temperature trend, and that CESM1’s 11-50 year av-
691 erage response to abrupt quadrupling of CO₂ is an appropriate tool with which to un-
692 derstand the models’ response to realistic, historical forcing. We then decompose the full
693 equatorial thermocline response into a response due to buoyancy forcing alone and mo-
694 mentum forcing alone, the latter of which drives thermocline cooling. We use an ocean-
695 only GCM with anomalous SST forcing to further decompose that buoyancy-forced com-
696 ponent, and we demonstrate that the response due to extratropical SST forcing and trop-
697 ical SST forcing linearly combine to recreate the full field buoyancy-forced response. The
698 remote, extratropically-driven response leads to a coherent thermocline warming through
699 dynamic and thermodynamic pathways. The increase in near-surface stratification in the
700 local, tropically-driven response leads to both a shoaling thermocline and a relaxation
701 of thermocline tilt. Our primary finding is that a simple linear combination of these ad-
702 justments, i) momentum-driven, ii) remote buoyancy-driven, and iii) local buoyancy-driven,
703 skillfully explains both the long-term 1958-2020 modeled and observed responses. We
704 can attribute certain features of the pattern to certain dynamics: we agree with Vecchi
705 and Soden (2007) and Jiang et al. (2025)’s suggestion that the thermocline cooling re-
706 sponse to global warming results from momentum-driven dynamics. However, this dy-
707 namical understanding does not explain more recent trends (e.g., the 1979-2020 response),
708 suggesting that this period was strongly affected by internal variability.

709 Our results emphasize that the subsurface equatorial Pacific temperature response
710 to climate change is a highly linear system. This linearity is powerful. It allows us to test
711 long-held theoretical understandings, such as how subtropical warming will affect the tran-

712 sient adjustment of the tropical thermocline or that changes in zonal wind stress are nec-
713 essary for a thermocline tilt. While this study does not answer what has caused recent
714 subsurface mismatches between models and observations or whether models are miss-
715 ing a hypothetical forcing that might explain that mismatch, we demonstrate that model
716 mean states are not so irreparably biased that we cannot learn from them. Instead, these
717 models clarify the specific patterns created by commonly referenced ocean dynamic ad-
718 justments. In a practical sense, we also outline a clear model hierarchy, fully-coupled,
719 mechanically-decoupled, ocean-only, and reduced gravity, which could be potentially lever-
720 aged to comprehend other coupled climate responses.

721 **6 Open Research**

722 Observational temperature data (EN04 & Ishii: Good et al., 2013; Ishii & Kimoto,
723 2009) and ocean reanalysis data (ORAS5 & SODA2.2.4 Zuo et al., 2019; Carton & Giese,
724 2008) are available online from their respective sources. Large ensemble data are avail-
725 able online from the World Climate Research Programme Earth System Grid Federa-
726 tion node (<https://esgf-node.ornl.gov/search>). The CESM1 and MITgcm simu-
727 lation data considered in this study are available from Luongo (2026). Several of the CESM1
728 and MITgcm simulations were originally presented in Luongo et al. (2022), Taylor et al.
729 (2025), and Luongo et al. (2025). Python code for idealized global reduced gravity model
730 is available from Sun and Thompson (2020).

731 **7 Conflict of Interest Statement**

732 The authors have no conflicts of interest to disclose.

733 **Acknowledgments**

734 MTL was supported by the Cooperative Institute for Climate, Ocean, & Ecosystem Stud-
735 ies (CICOES) under NOAA Cooperative Agreement NA20OAR4320271, Contribution
736 No. 2026-1538. IE was supported by National Science Foundation (NSF) award OCE-
737 2048590. KCA was supported by NSF award AGS-2203543 and a Calvin Professorship
738 in Oceanography. We thank NSF NCAR for providing exploratory allocations of core
739 hours on the Cheyenne and Derecho supercomputers. We sincerely thank Feng Jiang for
740 providing the ensemble mean model data used in Figure 1b & d, and without implying
741 endorsement, we thank Natalie Burls for helpful discussion. We also thank our editor,

742 Dr. Xin Wang, and three anonymous reviewers for thoughtful and constructive feedback
743 that greatly improved this study.

744 **References**

- 745 Baldwin, J. W., Atwood, A. R., Vecchi, G. A., & Battisti, D. S. (2021). Outsize
746 Influence of Central American Orography on Global Climate. *AGU Advances*,
747 *2*(2), e2020AV000343.
- 748 Bjerknes, J. (1969). Atmospheric Teleconnections from the Equatorial Pacific.
749 *Monthly weather review*, *97*(3), 163–172.
- 750 Burls, N., & Fedorov, A. (2014). What Controls the Mean East–West Sea Surface
751 Temperature Gradient in the Equatorial Pacific: The Role of Cloud Albedo.
752 *Journal of Climate*, *27*(7), 2757–2778.
- 753 Capotondi, A., McGregor, S., McPhaden, M. J., Cravatte, S., Holbrook, N. J.,
754 Imada, Y., ... others (2023). Mechanisms of Tropical Pacific Decadal Variabil-
755 ity. *Nature Reviews Earth & Environment*, *4*(11), 754–769.
- 756 Carton, J. A., & Giese, B. S. (2008). A Reanalysis of Ocean Climate Using Sim-
757 ple Ocean Data Assimilation (SODA). *Monthly weather review*, *136*(8), 2999–
758 3017.
- 759 Clement, A. C., Seager, R., Cane, M. A., & Zebiak, S. E. (1996). An Ocean Dynam-
760 ical Thermostat. *Journal of Climate*, *9*(9), 2190–2196.
- 761 Coats, S., & Karnauskas, K. (2017). Are Simulated and Observed Twentieth Cen-
762 tury Tropical Pacific Sea Surface Temperature Trends Significant Relative to
763 Internal Variability? *Geophysical Research Letters*, *44*(19), 9928–9937.
- 764 Dhame, S., Olonscheck, D., & Rugenstein, M. (2025). Higher-Resolution Climate
765 Models Do Not Consistently Reproduce the Observed Tropical Pacific Warm-
766 ing Pattern. *Journal of Climate*, *38*(13), 3131–3149.
- 767 DiNezio, P. N., Clement, A. C., Vecchi, G. A., Soden, B. J., Kirtman, B. P., & Lee,
768 S.-K. (2009). Climate Response of the Equatorial Pacific to Global Warming.
769 *Journal of Climate*, *22*(18), 4873–4892.
- 770 Dong, Y., Armour, K. C., Battisti, D. S., & Blanchard-Wrigglesworth, E. (2022).
771 Two-way Teleconnections between the Southern Ocean and the Tropical Pa-
772 cific via a Dynamic Feedback. *Journal of Climate*, *35*(19), 6267–6282.
- 773 Forget, G., Campin, J.-M., Heimbach, P., Hill, C., Ponte, R., & Wunsch, C. (2015).
774 ECCO Version 4: An Integrated Framework for Non-Linear Inverse Modeling

- 775 and Global Ocean State Estimation. *Geoscientific Model Development*, 8(10),
776 3071–3104.
- 777 Good, S. A., Martin, M. J., & Rayner, N. A. (2013). EN4: Quality Controlled
778 Ocean Temperature and Salinity Profiles and Monthly Objective Analyses with
779 Uncertainty Estimates. *Journal of Geophysical Research: Oceans*, 118(12),
780 6704–6716.
- Heede, U. K., & Fedorov, A. V. (2021). Eastern Equatorial Pa-
cific Warming Delayed by Aerosols and Thermostat Response to
CO₂ Increase. *Nature Climate Change*, 11(8), 696 – –703.
- 781 Heede, U. K., & Fedorov, A. V. (2023). Colder Eastern Equatorial Pacific and
782 Stronger Walker Circulation in the Early 21st Century: Separating the Forced
783 Response to Global Warming from Natural Variability. *Geophysical Research*
784 *Letters*, 50(3), e2022GL101020.
- 785 Heede, U. K., Fedorov, A. V., & Burls, N. J. (2020). Time Scales and Mechanisms
786 for the Tropical Pacific Response to Global Warming: A Tug of War between
787 the Ocean Thermostat and Weaker Walker. *Journal of Climate*, 33(14), 6101–
788 6118.
- 789 Heede, U. K., Fedorov, A. V., & Burls, N. J. (2021). A Stronger versus Weaker
790 Walker: Understanding Model Differences in Fast and Slow Tropical Pacific
791 Responses to Global Warming. *Climate Dynamics*, 57(9), 2505–2522.
- 792 Horel, J. D., & Wallace, J. M. (1981). Planetary-scale Atmospheric Phenomena As-
793 sociated with the Southern Oscillation. *Monthly Weather Review*, 109(4), 813–
794 829.
- 795 Hurrell, J. W., Holland, M. M., Gent, P. R., Ghan, S., Kay, J. E., Kushner, P. J.,
796 ... others (2013). The Community Earth System Model: A Framework for
797 Collaborative Research. *Bulletin of the American Meteorological Society*,
798 94(9), 1339–1360.
- 799 Hwang, Y.-T., Xie, S.-P., Chen, P.-J., Tseng, H.-Y., & Deser, C. (2024). Contri-
800 bution of Anthropogenic Aerosols to Persistent La Niña-like Conditions in the
801 Early 21st Century. *Proceedings of the National Academy of Sciences*, 121(5),
802 e2315124121.
- 803 Ishii, M., & Kimoto, M. (2009). Reevaluation of Historical Ocean Heat Content
804 Variations with Time-Varying XBT and MBT Depth Bias Corrections. *Journal*

- 805 *of Oceanography*, 65(3), 287–299.
- 806 Jiang, F., Seager, R., & Cane, M. A. (2024a). A Climate Change Signal in the Trop-
807 ical Pacific Emerges from Decadal Variability. *Nature Communications*, 15(1),
808 8291.
- 809 Jiang, F., Seager, R., & Cane, M. A. (2024b). Historical Subsurface Cooling in the
810 Tropical Pacific and its Dynamics. *Journal of Climate*, 37(22), 5925–5938.
- 811 Jiang, F., Seager, R., Cane, M. A., Karamperidou, C., & Brizuela, N. G. (2025).
812 Subsurface Cooling and Sea Surface Temperature Pattern Formation over
813 the Equatorial Pacific. *Journal of Geophysical Research: Oceans*, 130(4),
814 e2024JC022222.
- 815 Ju, W.-S., Zhang, Y., & Du, Y. (2022). Subsurface Cooling in the Tropical Pacific
816 under a Warming Climate. *Journal of Geophysical Research: Oceans*, 127(5),
817 e2021JC018225.
- 818 Kang, S. M., Hawcroft, M., Xiang, B., Hwang, Y.-T., Cazes, G., Codron, F., . . .
819 others (2019). Extratropical–Tropical Interaction Model Intercomparison
820 Project (ETIN-MIP): Protocol and Initial Results. *Bulletin of the American*
821 *Meteorological Society*, 100(12), 2589–2606.
- 822 Kang, S. M., Held, I. M., Frierson, D. M., & Zhao, M. (2008). The Response of the
823 ITCZ to Extratropical Thermal Forcing: Idealized Slab-Ocean Experiments
824 with a GCM. *Journal of Climate*, 21(14), 3521–3532.
- 825 Kang, S. M., Shin, Y., Kim, H., Xie, S.-P., & Hu, S. (2023). Disentangling the
826 Mechanisms of Equatorial Pacific Climate Change. *Science Advances*, 9(19),
827 eadf5059.
- 828 Karnauskas, K. B., Seager, R., Kaplan, A., Kushnir, Y., & Cane, M. A. (2009).
829 Observed Strengthening of the Zonal Sea Surface Temperature Gradient across
830 the Equatorial Pacific Ocean. *Journal of Climate*, 22(16), 4316–4321.
- Knutson, T. R., & Manabe, S. (1995). Time-mean Response
over the Tropical Pacific to Increased CO₂ in a Coupled Ocean
–
Atmosphere Model. Journal of Climate, 8(9), 2181 – 2199.
- 831 Kosaka, Y., & Xie, S.-P. (2016). The Tropical Pacific as a Key Pacemaker of the
832 Variable Rates of Global Warming. *Nature Geoscience*, 9(9), 669–673.
- 833 Laepple, T., & Huybers, P. (2014). Ocean Surface Temperature Variability: Large
834 Model-Data Differences at Decadal and Longer Periods. *Proceedings of the Na-*

- 835 *tional Academy of Sciences*, 111(47), 16682–16687.
- 836 Liu, Z. (1994). A Simple Model of the Mass Exchange between the Subtropical and
837 Tropical Ocean. *Journal of Physical Oceanography*, 24(6), 1153–1165.
- 838 Luo, Y., Liu, F., & Lu, J. (2018). Response of the Equatorial Pacific Thermocline to
839 Climate Warming. *Ocean Dynamics*, 68(11), 1419–1429.
- 840 Luo, Y., Lu, J., Liu, F., & Garuba, O. (2017). The Role of Ocean Dynamical Ther-
841 mostat in Delaying the El Niño-like Response over the Equatorial Pacific to
842 Climate Warming. *Journal of Climate*, 30(8), 2811–2827.
- 843 Luo, Y., Rothstein, L. M., & Zhang, R.-H. (2009). Response of Pacific Subtropical-
844 Tropical Thermocline Water Pathways and Transports to Global Warming.
845 *Geophysical Research Letters*, 36(4).
- 846 Luongo, M. T. (2026). *Data from Luongo et al. (2026): "Explaining the Equatorial*
847 *Pacific Thermocline Response to Climate Change with a Model Hierarchy"*.
848 Version 1, Dataset: <https://zenodo.org/records/19058074>. Zenodo. doi:
849 10.5281/zenodo.19058074
- 850 Luongo, M. T., Brizuela, N. G., Eisenman, I., & Xie, S.-P. (2024). Retaining
851 Short-term Variability Reduces Mean State Biases in Wind Stress Overrid-
852 ing Simulations. *Journal of Advances in Modeling Earth Systems*, 16(2),
853 e2023MS003665.
- 854 Luongo, M. T., Xie, S.-P., & Eisenman, I. (2022). Buoyancy forcing dominates
855 the cross-equatorial ocean heat transport response to Northern Hemisphere
856 extratropical cooling. *Journal of Climate*, 35(20), 6671–6690.
- 857 Luongo, M. T., Xie, S.-P., Eisenman, I., Hwang, Y.-T., & Tseng, H.-Y. (2023). A
858 Pathway for Northern Hemisphere Extratropical Cooling to Elicit a Tropical
859 Response. *Geophysical Research Letters*, 50(2), e2022GL100719.
- 860 Luongo, M. T., Xie, S.-P., Eisenman, I., Sun, S., & Peng, Q. (2025). How the Sub-
861 surface Tropical Pacific Responds to Subtropical Surface Cooling: Implications
862 for Cross-Equatorial Transport. *Journal of Climate*.
- 863 L’Heureux, M. L., Lee, S., & Lyon, B. (2013). Recent Multidecadal Strengthening
864 of the Walker Circulation across the Tropical Pacific. *Nature Climate Change*,
865 3(6), 571–576.
- 866 Mantua, N. J., Hare, S. R., Zhang, Y., Wallace, J. M., & Francis, R. C. (1997). A
867 Pacific Interdecadal Climate Oscillation with Impacts on Salmon Production.

- 868 *Bulletin of the American Meteorological Society*, 78(6), 1069–1080.
- 869 McCreary Jr, J. P., & Lu, P. (1994). Interaction between the Subtropical and Equatorial
870 Ocean Circulations: The Subtropical Cell. *Journal of Physical Oceanography*, 24(2), 466–497.
- 871
- 872 McGregor, S., Stuecker, M. F., Kajtar, J. B., England, M. H., & Collins, M. (2018).
873 Model Tropical Atlantic Biases Underpin Diminished Pacific Decadal Variability.
874 *Nature Climate Change*, 8(6), 493–498.
- 875 Merlis, T. M., & Schneider, T. (2011). Changes in Zonal Surface Temperature Gradients
876 and Walker Circulations in a Wide Range of Climates. *Journal of Climate*, 24(17), 4757–4768.
- 877
- 878 Olonscheck, D., Rugenstein, M., & Marotzke, J. (2020). Broad Consistency between
879 Observed and Simulated Trends in Sea Surface Temperature Patterns. *Geophysical Research Letters*, 47(10), e2019GL086773.
- 880
- 881 Peng, Q., Xie, S.-P., Wang, D., Huang, R. X., Chen, G., Shu, Y., . . . Liu, W. (2022).
882 Surface Warming-Induced Global Acceleration of Upper Ocean Currents. *Science Advances*, 8(16), eabj8394.
- 883
- 884 Philander, S. G. H. (1983). El Niño Southern Oscillation Phenomena. *Nature*,
885 302(5906), 295–301.
- 886 Seager, R., Cane, M., Henderson, N., Lee, D.-E., Abernathey, R., & Zhang, H.
887 (2019). Strengthening Tropical Pacific Zonal Sea Surface Temperature Gradient
888 Consistent with Rising Greenhouse Gases. *Nature Climate Change*, 9(7),
889 517–522.
- 890 Seager, R., Henderson, N., & Cane, M. (2022). Persistent Discrepancies between
891 Observed and Modeled Trends in the Tropical Pacific Ocean. *Journal of Climate*,
892 35(14), 4571–4584.
- 893 Seager, R., & Murtugudde, R. (1997). Ocean Dynamics, Thermocline Adjustment,
894 and Regulation of Tropical SST. *Journal of Climate*, 10(3), 521–534.
- 895 Solomon, A., & Newman, M. (2012). Reconciling Disparate Twentieth-century Indo-
896 Pacific Ocean Temperature Trends in the Instrumental Record. *Nature Climate
897 Change*, 2(9), 691–699.
- 898 Sun, S., & Thompson, A. F. (2020). Centennial Changes in the Indonesian Through-
899 flow Connected to the Atlantic Meridional Overturning Circulation: The
900 Ocean’s Transient Conveyor Belt. *Geophysical Research Letters*, 47(21),

- 901 e2020GL090615.
- 902 Sweeney, A. J., Fu, Q., Po-Chedley, S., Wang, H., & Wang, M. (2023). Internal Vari-
 903 ability Increased Arctic Amplification during 1980–2022. *Geophysical Research*
 904 *Letters*, *50*(24), e2023GL106060.
- 905 Taylor, B. A., Shi, J.-R., Xie, S.-P., Talley, L. D., Luongo, M. T., & Peng, Q. (2025).
 906 Warming Band in Southern Ocean’s Indian Sector: The Role of Remote At-
 907 lantic Buoyancy Forcing via Poleward-Shifting Circulation Response. *Journal*
 908 *of Climate*, *38*(14), 3219–3238.
- 909 Tseng, H.-Y., Hwang, Y.-T., Xie, S.-P., Tseng, Y.-H., Kang, S. M., Luongo, M. T.,
 910 & Eisenman, I. (2023). Fast and Slow Responses of the Tropical Pacific to
 911 Radiative Forcing in Northern High Latitudes. *Journal of Climate*, *36*(16),
 912 5337–5349.
- 913 Tuchen, F. P., Perez, R. C., Foltz, G. R., McPhaden, M. J., & Lumpkin, R. (2024).
 914 Strengthening of the Equatorial Pacific Upper-Ocean Circulation over the
 915 Past Three Decades. *Journal of Geophysical Research: Oceans*, *129*(11),
 916 e2024JC021343.
- 917 Vecchi, G. A., & Soden, B. J. (2007). Global Warming and the Weakening of the
 918 Tropical Circulation. *Journal of Climate*, *20*(17), 4316–4340.
- 919 Watanabe, M., Dufresne, J.-L., Kosaka, Y., Mauritsen, T., & Tatebe, H. (2021). En-
 920 hanced Warming Constrained by Past Trends in Equatorial Pacific Sea Surface
 921 Temperature Gradient. *Nature Climate Change*, *11*(1), 33–37.
- 922 Watanabe, M., Kang, S. M., Collins, M., Hwang, Y.-T., McGregor, S., & Stuecker,
 923 M. F. (2024). Possible Shift in Controls of the Tropical Pacific Surface Warm-
 924 ing Pattern. *Nature*, *630*(8016), 315–324.
- 925 Wills, R. C., Dong, Y., Proistosescu, C., Armour, K. C., & Battisti, D. S. (2022).
 926 Systematic Climate Model Biases in the Large-scale Patterns of Recent Sea-
 927 surface Temperature and Sea-level Pressure Change. *Geophysical Research*
 928 *Letters*, *49*(17), e2022GL100011.
- 929 Wyrтки, K. (1975). El Niño—The Dynamic Response of the Equatorial Pacific
 930 Ocean to Atmospheric Forcing. *Journal of Physical Oceanography*, *5*(4), 572–
 931 584.
- 932 Xie, S.-P., Deser, C., Vecchi, G. A., Ma, J., Teng, H., & Wittenberg, A. T. (2010).
 933 Global Warming Pattern Formation: Sea Surface Temperature and Rainfall.

934 *Journal of Climate*, 23(4), 966–986.

935 Yang, H., Wang, F., & Sun, A. (2009). Understanding the ocean temperature change
936 in global warming: the tropical Pacific. *Tellus A: Dynamic Meteorology and*

937 *Oceanography*, 61(3), 371–380.

938 Zuo, H., Balmaseda, M. A., Tietsche, S., Mogensen, K., & Mayer, M. (2019). The
939 ECMWF Operational Ensemble Reanalysis–Analysis System for Ocean and

940 Sea Ice: A Description of the System and Assessment. *Ocean science*, 15(3),

941 779–808.

Supporting Information for “Explaining the Equatorial Pacific Thermocline Response to Climate Change with a Model Hierarchy”

Matthew T. Luongo^{1,2}, Shang-Ping Xie³, Ian Eisenman³, Shantong Sun⁴, &
Kyle C. Armour^{2,5}

¹Cooperative Institute for Climate, Ocean, & Ecosystem Studies, University of Washington, Seattle, WA

²School of Oceanography, University of Washington, Seattle, WA

³Scripps Institution of Oceanography, UC San Diego, La Jolla, CA

⁴Laoshan Laboratory, Qingdao, China

⁵Department of Atmospheric & Climate Science, University of Washington, Seattle, WA

Contents of this file Table S1 and Figures S1-S6.

References

- Carton, J. A., & Giese, B. S. (2008). A Reanalysis of Ocean Climate Using Simple Ocean Data Assimilation (SODA). *Monthly weather review*, *136*(8), 2999–3017.
- Good, S. A., Martin, M. J., & Rayner, N. A. (2013). EN4: Quality Controlled Ocean Temperature and Salinity Profiles and Monthly Objective Analyses with Uncertainty Estimates. *Journal of Geophysical Research: Oceans*, *118*(12), 6704–6716.
- Ishii, M., & Kimoto, M. (2009). Reevaluation of Historical Ocean Heat Content Variations with Time-Varying XBT and MBT Depth Bias Corrections. *Journal of Oceanography*, *65*(3), 287–299.

- Jiang, F., Seager, R., Cane, M. A., Karamperidou, C., & Brizuela, N. G. (2025). Subsurface Cooling and Sea Surface Temperature Pattern Formation over the Equatorial Pacific. *Journal of Geophysical Research: Oceans*, *130*(4), e2024JC022222.
- Kang, S. M., Hawcroft, M., Xiang, B., Hwang, Y.-T., Cazes, G., Codron, F., . . . others (2019). Extratropical–Tropical Interaction Model Intercomparison Project (ETIN-MIP): Protocol and Initial Results. *Bulletin of the American Meteorological Society*, *100*(12), 2589–2606.
- Zuo, H., Balmaseda, M. A., Tietsche, S., Mogensen, K., & Mayer, M. (2019). The ECMWF Operational Ensemble Reanalysis–Analysis System for Ocean and Sea Ice: A Description of the System and Assessment. *Ocean science*, *15*(3), 779–808.

| Fully-coupled Simulations | | | |
|------------------------------------|-----------------------------------|--------------------|-----------------|
| Simulation Name | CO ₂ Forcing | Wind Stress | ETINMIP Forcing |
| ETINMIPNH | 280ppm | Freely evolving | 45°N–65°N |
| ETINMIPSH | 280ppm | Freely evolving | 45°S–65°S |
| Mechanically-decoupled Simulations | | | |
| Simulation Name | CO ₂ Forcing | Wind Stress | ETINMIP Forcing |
| Tau.1.S.NH | 280ppm | Ctrl | 45°N–65°N |
| Tau.NH.S.1 | 280ppm | ETINMIPNH | n/a |
| Tau.1.S.SH | 280ppm | Ctrl | 45°S–65°S |
| Tau.SH.S.1 | 280ppm | ETINMIPSH | n/a |
| Ocean-only Simulations | | | |
| Simulation Name | SST Forcing Perturbation | SST Forcing Bounds | |
| ETINMIPNH_BFsst | Tau.1.S.NH-Tau1CO ₂ x1 | 90°S-90°N | |
| ETINMIPNH_BFsstET | Tau.1.S.NH-Tau1CO ₂ x1 | 90°S-6°S, 6°N-90°N | |
| ETINMIPNH_BFsstEQ | Tau.1.S.NH-Tau1CO ₂ x1 | 10°S-10°N | |
| ETINMIPSH_BFsst | Tau.1.S.SH-Tau1CO ₂ x1 | 90°S-90°N | |
| ETINMIPSH_BFsstET | Tau.1.S.SH-Tau1CO ₂ x1 | 90°S-6°S, 6°N-90°N | |
| ETINMIPSH_BFsstEQ | Tau.1.S.SH-Tau1CO ₂ x1 | 10°S-10°N | |

Table S1. Details of fully coupled, mechanically-decoupled, and ocean-only simulations using top-of-atmosphere hemispherically asymmetric extratropical forcing from the Extratropical-Tropical Interaction Model Intercomparison Project (ETINMIP: Kang et al., 2019). The Ctrl and Tau1CO₂x1 simulations are described in Table 1 of the main text.

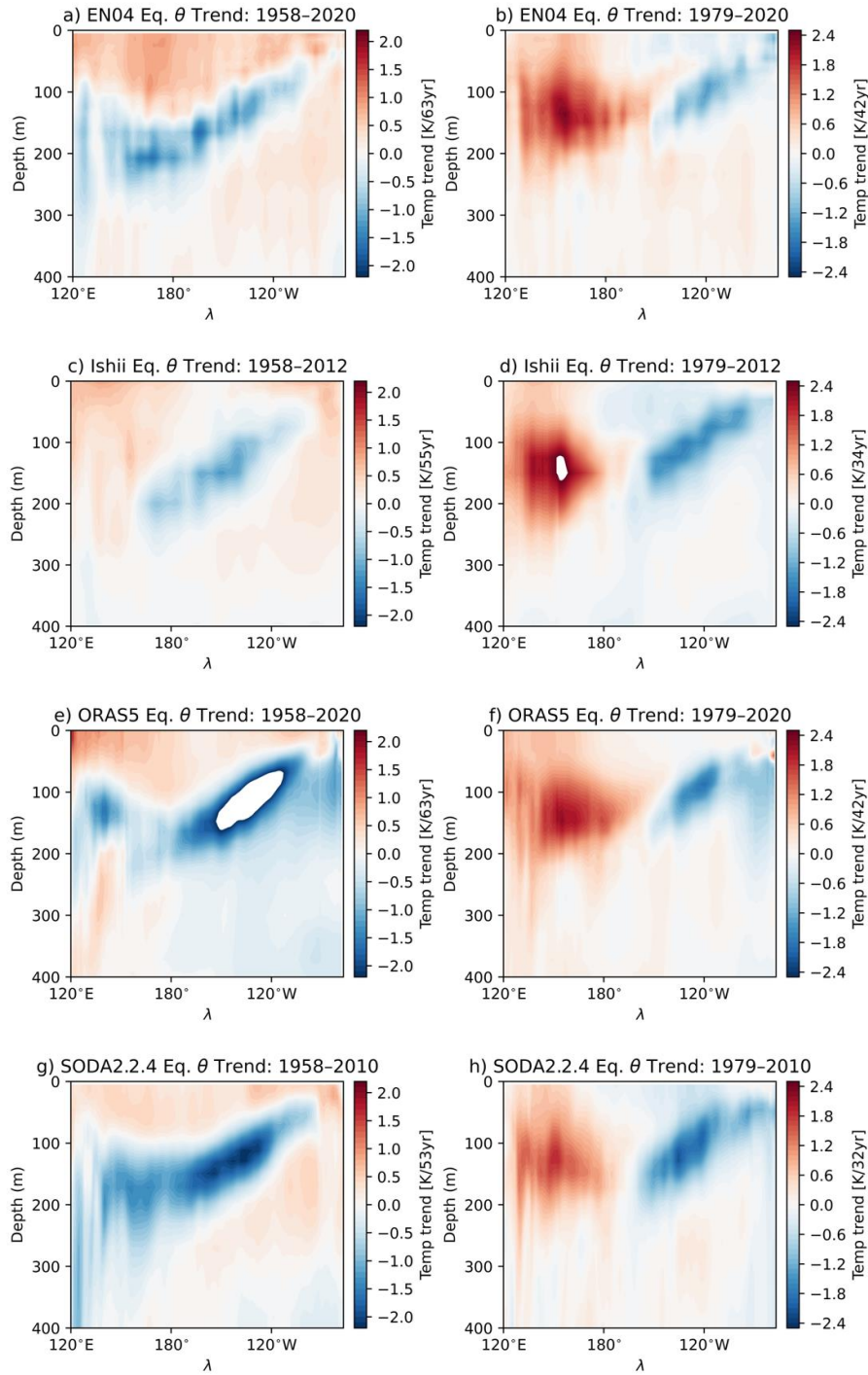


Figure S1. Equatorial subsurface temperature (θ) trend for EN04 observational product (top row, Good et al., 2013), Ishii observational product (second row, Ishii & Kimoto, 2009), ORAS5 ocean reanalysis (third row, Zuo et al., 2019), and SODA2.2.4 ocean reanalysis (fourth row, Carton & Giese, 2008) While time periods depend on specific data source, longer-term trends are in the left column and shorter-term trends in the right column.

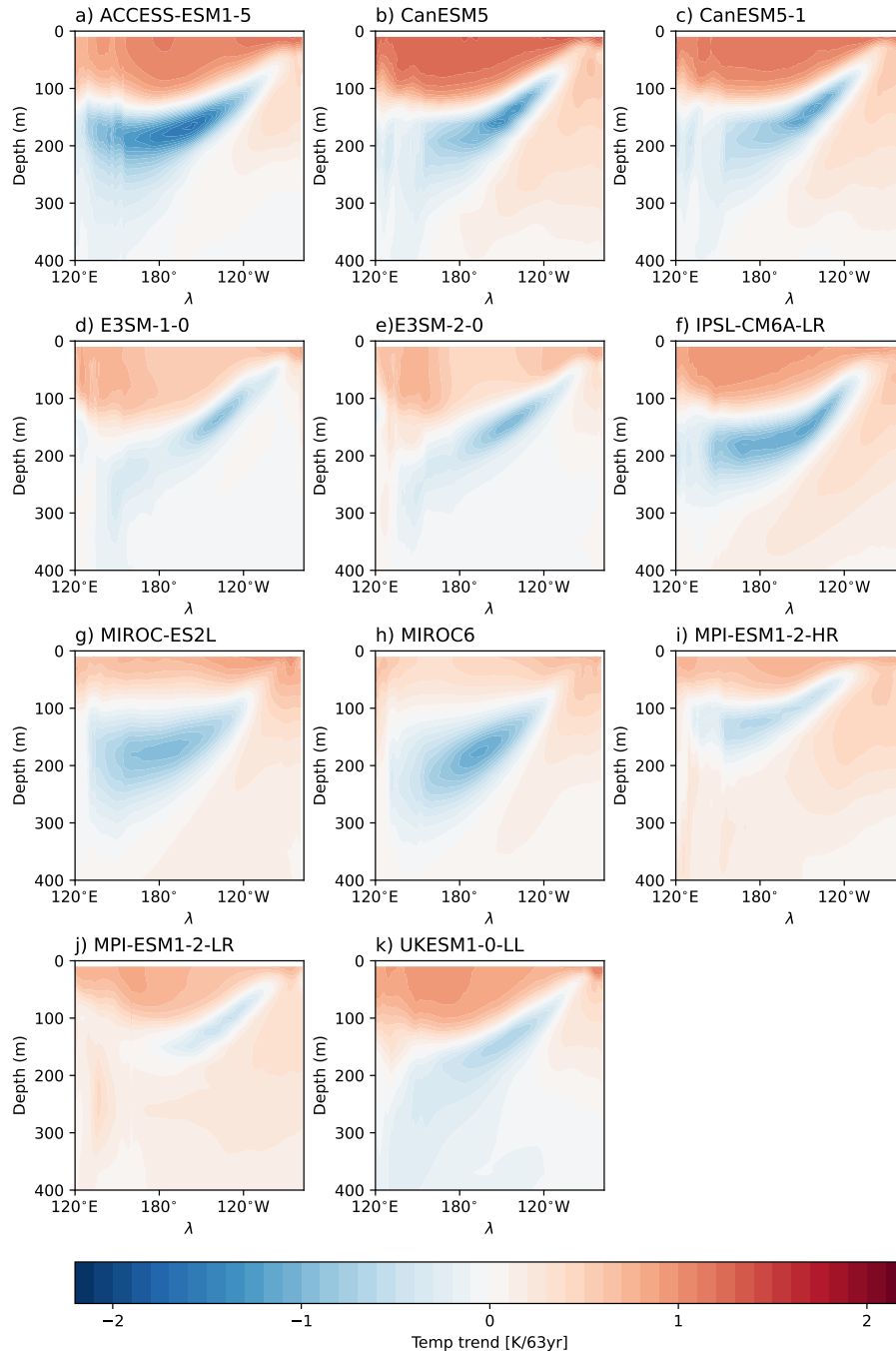


Figure S2. Ensemble mean 1958-2020 equatorial subsurface temperature (θ) trend for a) ACCESS-ESM1-5, b) CanESM5, c) CanESM5-1, d) E3SM-1-0, e) E3SM-2-0, f) IPSL-CM6A-LR, g) MIROC-ES2L, h) MIROC6, i) MPI-ESM1-2-HR, j) MPI-ESM1-2-LR, and k) UKESM1-0-LL large ensembles as selected by Jiang et al. (2025). Ensembles are forced by historical forcing from 1958-2014 and from 2015-2020 by the Shared Socioeconomic Pathway 3-7.5 scenario.

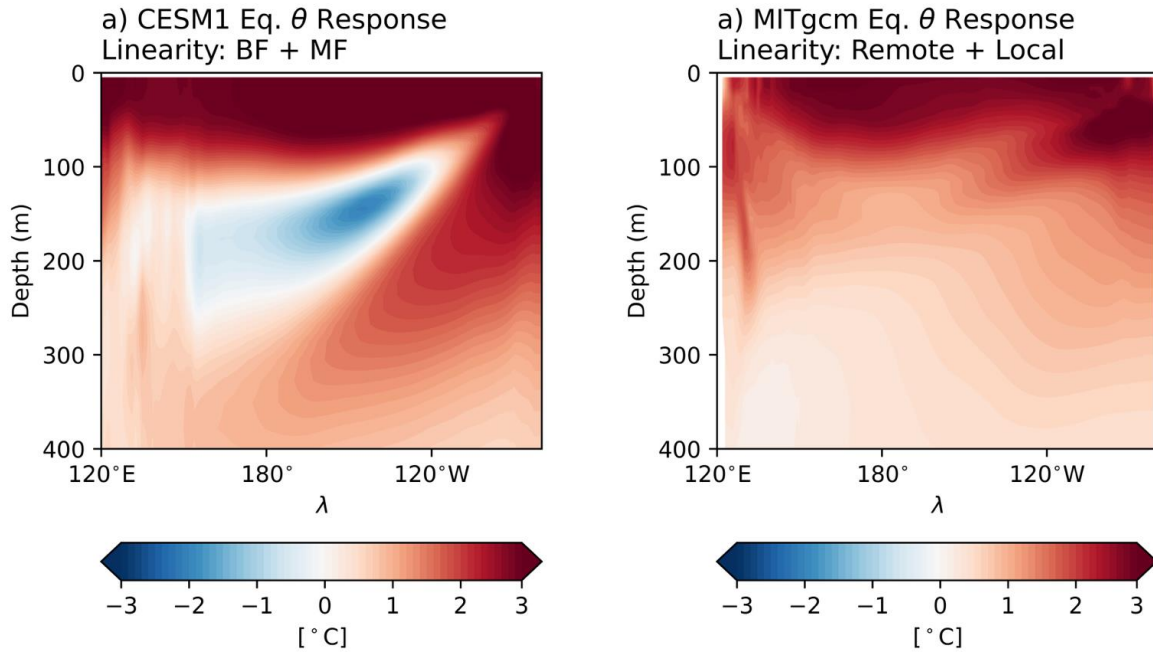


Figure S3. a) Linearity of CESM1 equatorial temperature (θ) response to abrupt quadrupling of CO_2 : Sum of buoyancy-forced ($\text{BF} = \text{Tau1CO}_2\text{x4} - \text{Tau1CO}_2\text{x1}$, Figure 2b of the main text) response and momentum-forced ($\text{MF} = \text{Tau4CO}_2\text{x1} - \text{Tau1CO}_2\text{x1}$, Figure 2c of the main text) response. Compare this sum with the FC response (Figure 2a of the main text). b) Linearity of the MITgcm equatorial θ response to BF SST forcing: Sum of response to remote SST forcing ($\text{CO}_2\text{x4_BFsstET-Octrl}$, Figure 4c of the main text) and response to local SST forcing ($\text{CO}_2\text{x4_BFsstEQ-Octrl}$, Figure 4d of the main text). Compare this sum with the full field response (Figure 3b of the main text).

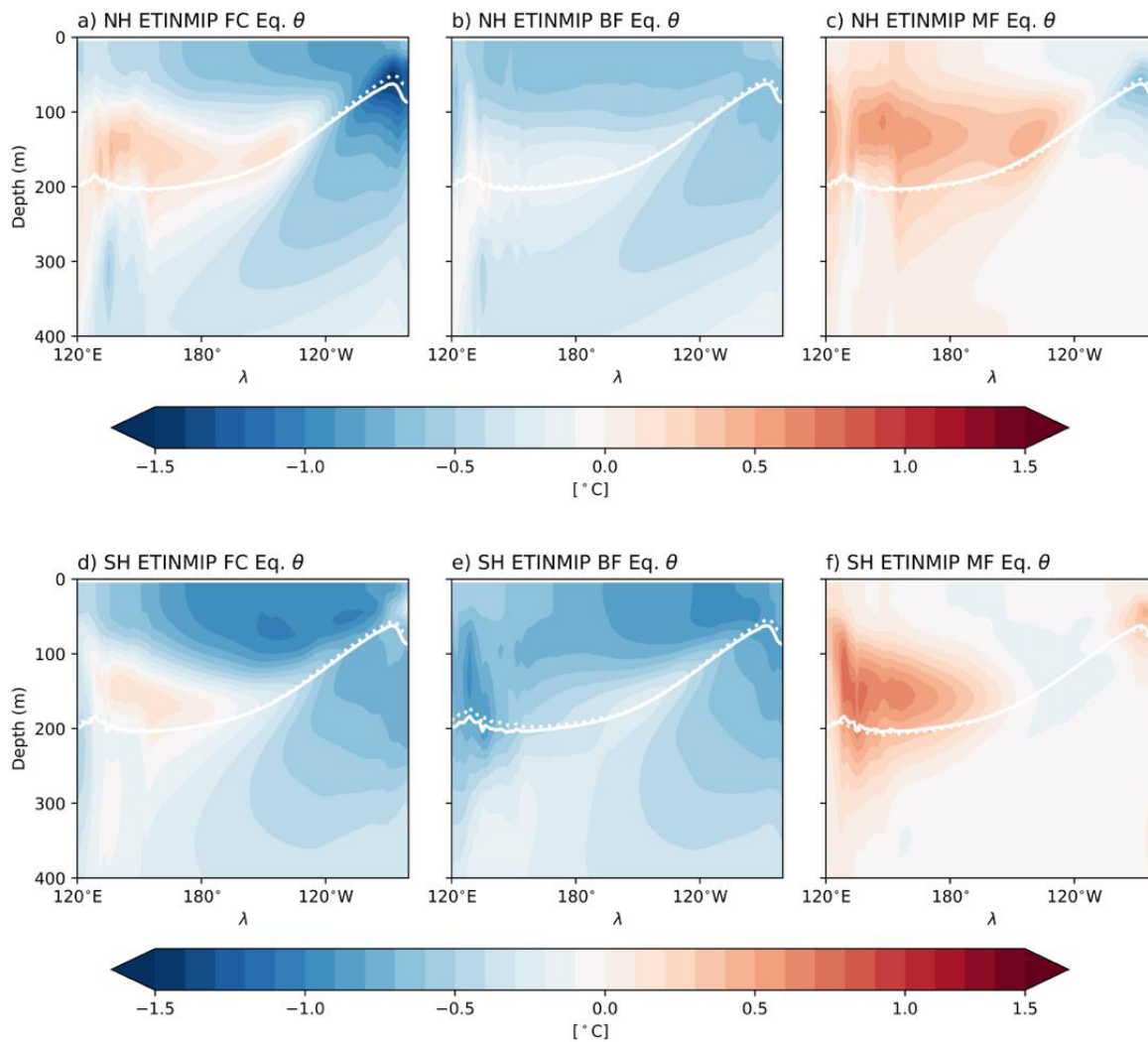


Figure S4. a) CESM1 fully-coupled (FC = ETINMIPNH-Ctrl) equatorial temperature (θ) response to Northern Hemisphere (NH) ETINMIP forcing. b) CESM1 buoyancy-forced (BF = Tau.1.S.NH-Tau1CO₂x1) equatorial θ response to NH ETINMIP forcing. c) CESM1 momentum-forced (MF = Tau.NH.S.1-Tau1CO₂x1) equatorial θ response to NH ETINMIP forcing. d) CESM1 FC (ETINMIPSH-Ctrl) equatorial θ response to Southern Hemisphere (SH) ETINMIP forcing. e) CESM1 BF (Tau.1.S.SH-Tau1CO₂x1) equatorial θ response to SH ETINMIP forcing. f) CESM1 MF (Tau.SH.S.1-Tau1CO₂x1) equatorial θ response to SH ETINMIP forcing. All panels are meridionally averaged from 5°S-5°N and temporally averaged from years 11-50. The 16°C isotherm from Ctrl is plotted as a solid white contour in all six panels and approximates the mean thermocline. Dotted white contours are the 16°C isotherm in the corresponding forced experiments.

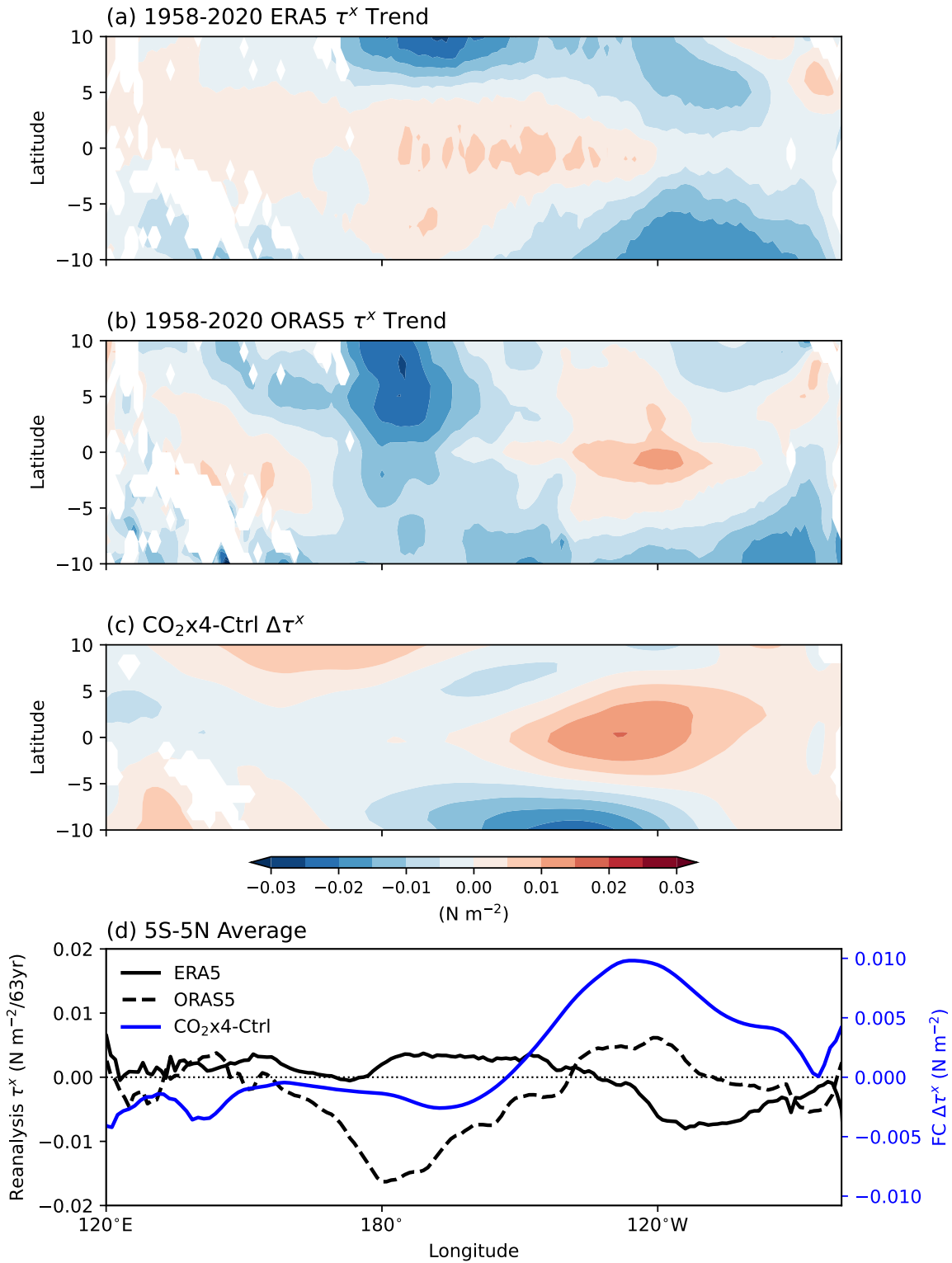


Figure S5. a) Equatorial Pacific 1958-2020 zonal wind stress (τ^x) trend in European Centre for Medium-Range Weather Forecast's ERA5 atmospheric reanalysis product. b) Equatorial Pacific 1958-2020 τ^x trend in European Centre for Medium-Range Weather Forecast's ORAS5 oceanic reanalysis product. c) CESM1 fully-coupled (FC = CO₂x4-Ctrl) equatorial temperature τ^x response to abrupt CO₂ quadrupling. d) 5°S-5°N averages of panels a-c, with the left axis corresponding to the reanalysis trends and the right axis corresponding to the CESM response.

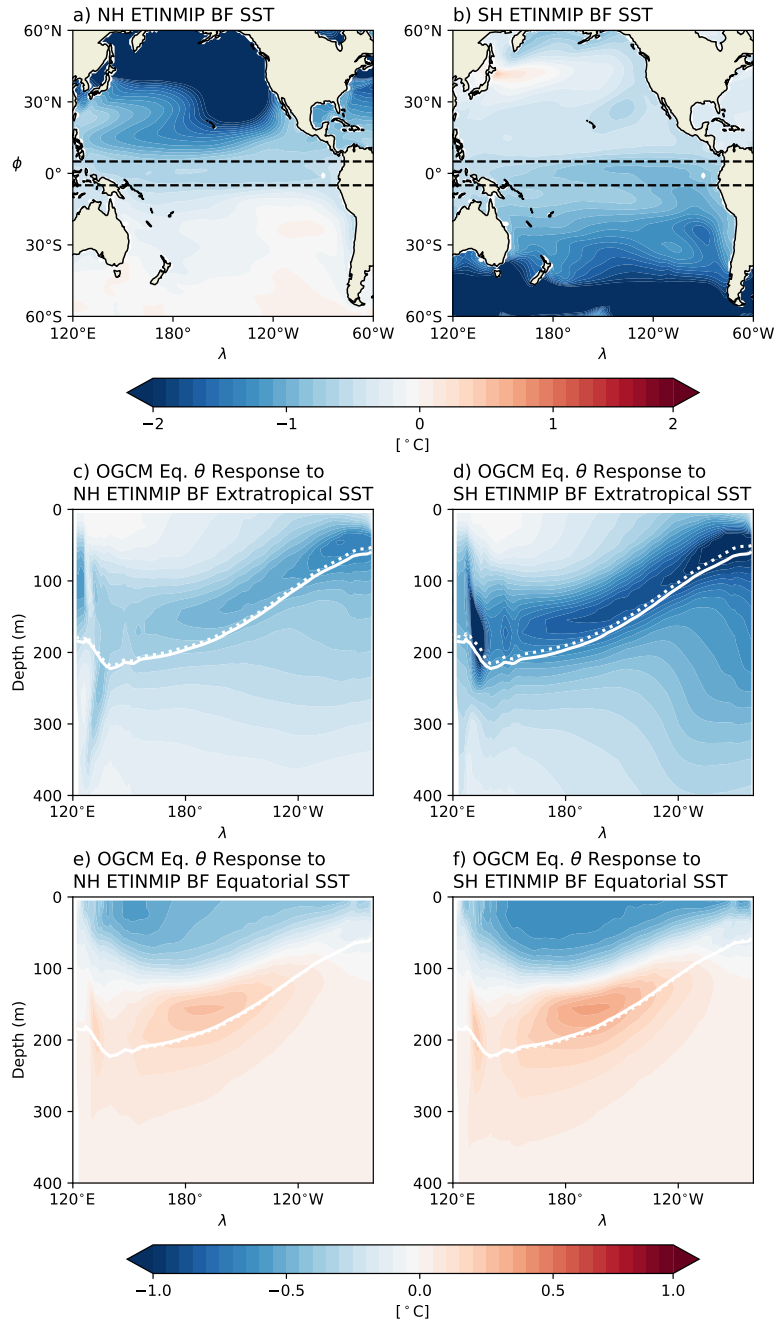


Figure S6. a) NH ETINMIP BF ($\text{Tau}_{1.S.NH}-\text{Tau}_{1\text{CO}_2\text{x1}}$) SST pattern from CESM1. b) SH ETINMIP BF ($\text{Tau}_{1.S.SH}-\text{Tau}_{1\text{CO}_2\text{x1}}$) SST pattern from CESM1. c) Equatorial θ response to remote NH ETINMIP BF SST forcing. d) Equatorial θ response to remote SH ETINMIP BF SST forcing. e) Equatorial θ response to local NH ETINMIP BF SST forcing. d) Equatorial θ response to local SH ETINMIP BF SST forcing. Dashed black lines in the top row correspond to the bounds that we separate the local and remote responses by. The 16°C isotherm in OCtrl (solid white contour in panels c-f) approximates the mean thermocline and the dashed white contour approximates the perturbed thermocline in respective forced simulations.

May 7, 2026, 6:44pm